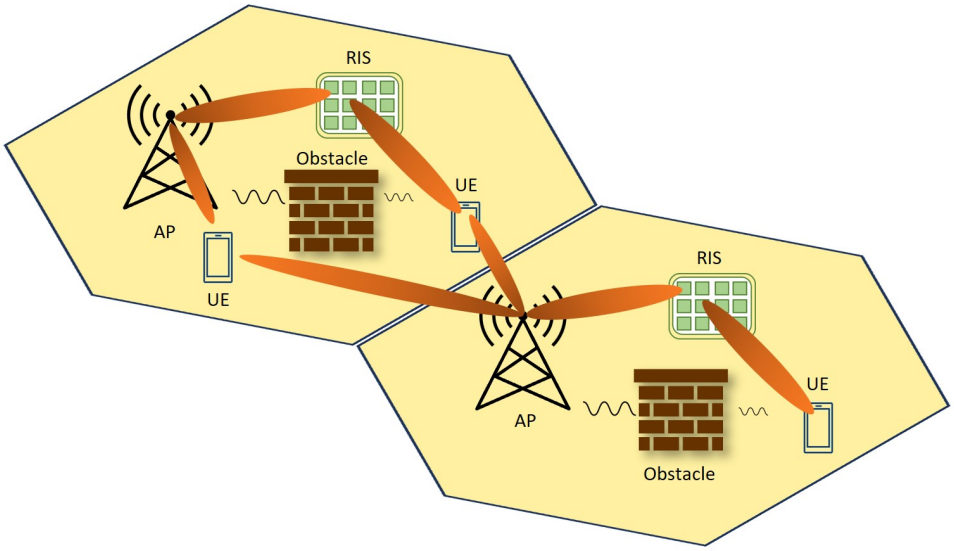

Integration of Reconfigurable Intelligent Surfaces (RISs) in D-MIMO Networks for 6G

A Chalmers University of Technology Master's thesis

Master's thesis in Masters Programme of Information and Communication Technology

AKSHAY VAYAL PARAMBATH

Department Of Electrical Engineering

CHALMERS UNIVERSITY OF TECHNOLOGY
Gothenburg, Sweden 2024
www.chalmers.se

Master's thesis 2024

Integration of Reconfigurable Intelligent Surfaces (RISs) in D-MIMO Networks for 6G

Akshay Vayal Parambath

Department of Electrical Engineering
Wireless Systems Division
Chalmers University of Technology
Gothenburg, Sweden 2024

Integration of Reconfigurable Intelligent Surfaces (RISs) in D-MIMO Networks for 6G
Akshay Vayal Parambath

Supervisors: Jose Flordelis, Fredrik Rusek, and Erik Bengtsson, Sony Research & Technology Center, Charitha Madapatha and Tommy Svensson, Chalmers
Examiner: Tommy Svensson, Department of Electrical Engineering, Chalmers

Master's Thesis 2024
Wireless Systems Division
Department of Electrical Engineering
Chalmers University of Technology
SE-412 96 Gothenburg
Telephone +46 31 772 1000

Cover: RIS integrated DMIMO model constructed in Matlab showing an indoor layout consisting of distributed APs, UEs, and RISs.

Typeset in LaTeX
Printed by Chalmers Reproservice
Gothenburg, Sweden 2024

Integration of Reconfigurable Intelligent Surfaces (RISs) in D-MIMO Networks for 6G

Akshay Vayal Parambath
Department of Electrical Engineering
Chalmers University of Technology

Abstract

The distributed MIMO (D-MIMO) systems are one of the potential technique to densify the ever-evolving 5G networks and beyond (6G) technologies. However, the scalability of D-MIMO systems to large-scale networks in a practical scenario is very challenging. The aim towards sustainability and other economic challenges in the upcoming 6G networks resulted in the exploitation of cost-effective and energy-efficient dynamic access point (AP) clustering techniques and use of densification enablers for providing high performance and reliability for its users. Reconfigurable intelligent surface (RIS) is a technology that is well known for its low-cost, rapid deployability, and energy-efficient properties, which can add extra diversity to the spatial domain if deployed in a network. This work explores the benefits gained by integrating RIS into a D-MIMO system in terms of major KPIs of focus, i.e., energy efficiency and service coverage of the system.

In this study, we focus an indoor use case with a high UE density where the service coverage is very scarce due to high obstacle density that results in huge pathloss and shadowing. Towards the end, we propose dynamic user-centric AP clustering and RIS placement techniques adapted for addressing such high UE demands in an indoor D-MIMO system. Here, for configuring RIS phase-shifts we use an alternating optimization method which is a sub-optimal solution to lower the computational complexity.

Finally, we compare an RIS-assisted D-MIMO system with a conventional D-MIMO system to prove that the integration of RISs in D-MIMO system is a potential approach to enhance the service coverage and energy efficiency, while satisfying the scalability requirement in 5G and beyond (6G) technologies.

Keywords: D-MIMO, RIS, User-centric AP clustering, Energy efficiency, Service coverage probability, 5G, 6G, Distributed MIMO.

Acknowledgements

I would like to thank my supervisor Professor Tommy Svensson for giving me the opportunity to work on this thesis and for his immense guidance, insights and support throughout this thesis work. A special thanks to my supervisor Charitha Madapatha for always being a support pillar during this thesis journey and for sharing his knowledge and valuable ideas which meant a lot during this research.
I would like to thank my supervisor Jose Flordelis from Sony Research & Technology Center for sharing his thoughts and valuable comments throughout this thesis work.
I also would like to extend my gratitude to Fredrik Rusek and Erik Bengtsson from Sony Research & Technology Center for their valuable comments and insights during this thesis.
The weekly scheduled meeting with all the supervisors helped me to learn and come up with new ideas, which improved our work at every stage of the project. The opportunity to be an internal part of the European level 6G flagship project Hexa-X-II was exciting and a huge responsibility at the same time. This really helped to boost my passion towards the research field. I am very grateful to everyone who made this possible.
A special thanks to my family and friends for their mental support throughout my educational journey and for uplifting me through the ups and downs in my life.

Akshay Vayal Parambath, Gothenburg, June 2024

List of Acronyms

Below is the list of acronyms that have been used throughout this thesis listed in numerical order followed by alphabetical order:

3GPP	3rd Generation Partnership Project
5G	5th Generation Mobile Network
6G	6th Generation Mobile Network
AP	Access Point
AWGN	Additive White Gaussian Noise
AI	Artificial Intelligence
BS	Base Station
CDF	Cumulative distribution function
CSI	Channel State Information
CSIT	Channel State Information at the Transmitter
CSIR	Channel State Information at the Receiver
D-MIMO	Distributed Multiple-Input And Multiple-Output
InH	Indoor Hotspot
LTE	Long-Term Evolution
LoS	Line-of-Sight
MIMO	Multiple-Input And Multiple-Output
ML	Machine Learning
NLoS	Non-Line-of-Sight
QSS	Queue-based Scheduling Scheme
RIS	Reconfigurable Intelligent Surfaces
SINR	Signal to Interference And Noise Ratio
SNR	Signal to Noise Ratio
SVD	Singular value decomposition
UE	User Equipment
UCS	Uniform Clustering Scheme

Nomenclature

Below is the nomenclature of indices, parameters, and variables that have been used throughout this thesis.

Indices

t	Timeslot for serving users
n,k,r	Indices for distribution of APs, UEs, and RISs respectively

Parameters

f_c	Carrier frequency
λ	Wavelength of the signal
c	Speed of light in vacuum
ξ	Inverse of the transmit amplifier efficiency
N_{AP}	Number of APs
N_{UE}	Number of UEs
N_{RIS}	Number of RIS elements
ζ_{AP}	AP cluster size
P_{T}	Transmit power at AP
P_{RX}	Received power by UE
I	Interference power at UE
P_{noise}	Noise power at UE
P_c	Static power consumption
Λ	UE density in an area
$\mathrm{Pr}_{\mathrm{LoS}}$	LoS probability between transmitter and receiver
$\mathrm{A}_{\mathrm{LoS}}$	LoS availability between transmitter and receiver
δ_{LoS}	LoS pathloss between transmitter and receiver

δ_{NLoS}	NLoS pathloss between transmitter and receiver
d	Euclidean distance between transmitter and receiver
d_{3D}	3D Euclidean distance between transmitter and receiver
R	AP-UE channel matrix
H	AP-RIS channel matrix
G	RIS-UE channel matrix
Φ	Phase-shift matrix of RIS
q	Unit-norm precoder vector of transmitter
w	Unit-norm combiner vector of UE
ε_{LoS}	Shadow fading in LoS path between the transmitter and receiver
$\varepsilon_{\text{NLoS}}$	Shadow fading in NLoS path between the transmitter and receiver
σ_{LoS}	Standard deviation of LoS shadow fading between the transmitter and receiver
σ_{NLoS}	Standard deviation of NLoS shadow fading between the transmitter and receiver
N	Number of iterations
η_{SE}	Spectral efficiency
η_{EE}	Energy efficiency
P_{c}	Static power consumption of whole system
$P_{\text{AP}_{\text{static}}}$	Static power consumption of an AP
$P_{\text{UE}_{\text{static}}}$	Static power consumption of a UE
P_{b}	Static power consumption of an RIS element
G_{TX}	Transmitter antenna gain
G_{RX}	Receiver antenna gain
G_{RIS}	RIS element gain
σ^2	Noise power at UE's receiver
F_{UE}	Noise figure for UE's receiver
R_{th}	Threshold data rate at UE

Variables

$P_{\text{RX}}(k, n, r)$	Power received by UE k from AP n and RIS r coordination
$R_{n,k}$	Data rate received by UE k from AP n
$H_{n,r}$	Channel matrix representing channel between AP n and RIS r

$G_{r,k}$	Channel matrix representing channel between RIS r and UE k
Φ_r	Phase matrix of RIS r
q_n	Precoder of AP n
w_k	Combiner of UE k

Contents

List of Acronyms **ix**

Nomenclature **xi**

List of Figures **xvii**

List of Tables **xix**

1 Introduction **1**
1.1 Background 1
1.1.1 Practical application 2
1.2 Aim 2
1.2.1 Limitations 2
1.2.2 Specification of the issues being investigated 3

2 Theory **5**
2.1 Wireless Communication 5
2.2 6G 6
2.3 Beamforming 6
2.4 Operational Frequency 7
2.5 D-MIMO 8
2.6 RIS 8
2.7 Channel Model 9
2.8 Pathloss 10
2.9 Service Coverage 10
2.10 Spectral Efficiency 11
2.11 Energy Efficiency 11

3 Methods **13**
3.1 System model 13
3.1.1 Deployment Model 13
3.1.1.1 D-MIMO deployment model for indoor layout 13
3.1.1.2 RIS integration in D-MIMO model for indoor layout 14
3.1.2 Channel model 15
3.1.2.1 Alternating optimization algorithm for joint precoding 16
3.1.2.2 AP-RIS-UE association and scheduling model 19
3.1.2.3 Uniform Power Allocation model 19

3.1.3 Measurement method 20
3.1.3.1 Received power and interference measurement 20
3.1.3.2 Signal-to-Interference-plus-Noise ratio (SINR) measurement 20
3.1.3.3 Data rate measurement 21
3.1.3.4 Service coverage probability measurement 21
3.1.3.5 Spectral efficiency and energy efficiency measurement 21

4 Results and discussions 23
4.1 Deployment Models 24
4.1.1 D-MIMO system model 24
4.1.2 RIS-assisted D-MIMO system model 24
4.2 Performance analysis 25
4.2.1 Analysis of optimal AP cluster size for D-MIMO system . . . 26
4.2.2 Enhancement in D-MIMO performance with RIS integration w.r.t. different AP cluster sizes 27
4.2.3 Performance analysis of different AP cluster sizes w.r.t. transmit power of AP for RIS-assisted D-MIMO system 28
4.2.4 Energy efficiency analysis of RIS-integrated D-MIMO system . 29
4.2.5 Service coverage probability analysis of RIS-assisted D-MIMO system 30

5 Conclusions 33

6 Future work 35

Bibliography 37

List of Figures

2.1 Wireless Communication model 6
2.2 Beamforming model 7
2.3 D-MIMO unit system 8
2.4 RIS unit model 9
2.5 RIS working model 9

3.1 D-MIMO system model 14
3.2 D-MIMO system unit model 14
3.3 RIS integrated D-MIMO system model 15
3.4 RIS integrated D-MIMO system unit model 15
3.5 Channel model of a single UE serving unit of D-MIMO with 2-AP and 1-RIS serving system. 17
3.6 RIS integrated D-MIMO system unit model representing a 4 AP cluster and 1 RIS serving an UE scenarios. 19

4.1 Deployment model of D-MIMO system. 24
4.2 Deployment model of RIS-assisted D-MIMO system. 25
4.3 SINR CDF comparison between conventional D-MIMO system with different AP cluster sizes i) 1, ii) 2, iii) 3, iv) 4, v) 5, and vi) 6 with $f_c = 4$ GHz, $B = 100$ MHz, and $P_T = 25$ dBm. 26
4.4 SINR CDF comparison between D-MIMO system with and without RIS for different AP cluster sizes i) 2 AP, ii) 3 AP, and iii) 4 AP with $f_c = 4$ GHz, $B = 100$ MHz, and $P_T = 25$ dBm. 27
4.5 SINR cdf comparison between to different AP cluster sizes for transmit powers i) $P_T = 25$ dBm, and ii) $P_T = 30$ dBm with $f_c = 4$ GHz, $B = 100$ MHz, $N_{RIS} = 128$, and $G_{RIS} = 4$ dB. 29
4.6 Energy efficiency analysis w.r.t. the number of RIS elements for RIS-integrated MIMO and D-MIMO models with $f_c = 4$ GHz, $B = 100$ MHz, $P_T = 25$ dBm, and $G_{RIS} = 4$ dB. 30
4.7 Service coverage probability analysis w.r.t. the number of RIS elements for MIMO and D-MIMO models with $f_c = 4$ GHz, $B = 100$ MHz, $P_T = 25$ dBm, and $G_{RIS} = 4$ dB. 31

List of Tables

4.1 System parameters 23
4.2 Median SINR of UEs analysis w.r.t. AP cluster size. 26

1
Introduction

1.1 Background

The continuous advancement in wireless communication aims to provide consistent performance and peak data rates to its users but most of the technologies lack incorporation of the energy efficiency factor during its development, which is crucial to promote sustainability. The 5th Generation (5G) mobile network and beyond technologies aim to build energy-efficient networks that can provide robust coverage and enhanced quality of service (QoS) to its users.

The replacement of the present MIMO network with the distributed MIMO (D-MIMO) network is one relevant solution that is capable of providing macro-diversity, which satisfies the two primary user requirements, i.e., expanded coverage area and higher QoS for robust connectivity [1]. D-MIMO system operates by coordinating several distributed radio units or access points (APs) in a particular geographical area using a common base station (BS). This strategy ensures that, all the users in the network are connected by at least one AP. However, some users in the D-MIMO network may fail to obtain service coverage due to the high pathloss, especially in an indoor scenario due to multiple stationary and mobile obstacles in the signal propagation path [2].

The use of network extenders like network-controlled repeaters (NCRs) and reconfigurable intelligent surfaces (RISs) in the D-MIMO network are the two potential approaches to overcome the pathloss issue and enhance service coverage. NCR is a repeater network capable of beamforming using amplify-and-forward operations, which can be controlled via specialized backhaul (BH) and access links [1]. RIS is a planar meshed metasurface with multiple passive reflective elements whose phase shifts can be independently altered using an intelligent controller. Both NCRs and RISs can redirect an RF signal toward the receiver's direction using beamforming and, therefore, are very beneficial when deployed in a network that lacks good service coverage. Unlike NCRs, RISs do not require any distinct access link or backhaul (BH) link to enable its beamforming ability and thus are more preferred as an energy-efficient choice. Therefore, deploying multiple RISs allows us to effectively sense and coordinate multiple APs to serve user equipments (UEs) in a D-MIMO system.

The significant advantages of using RISs include its low complexity and low-cost deployment properties, allowing it to be effortlessly integrated into an existing network by coating them on almost any infrastructure. Also, its ability to introduce multi-paths can be leveraged to enrich the channel, which in turn enhances the ser-

vice coverage of UEs if deployed in a network. Moreover, it is a sustainable network extender due to its passive nature.
Even though RISs help to sort out significant problems faced by the users in a D-MIMO network, it require channel state information (CSI) to align its phase-shifts for re-transmitting the signal towards a desired UE. In this research, we assume that CSI is already known to the transmitter to simplify the problem formulation and to effortlessly analyze a RIS-assisted D-MIMO system for investigating its benefits in performance improvement compared to a conventional D-MIMO system [3].

1.1.1 Practical application

The main practical use cases of integrating RISs into an indoor D-MIMO network include:

1. Provide centralized beamforming for improving the energy harvesting of the internet-of-things (IoT) devices in a network [4].
2. Support e-Health, especially in senior citizen healthcare, to sense if anyone is falling from their posture change leveraging the precise sensing property of RIS [5].
3. Sense and coordinate mobile robots inside factories to efficiently communicate with each other regardless of any signal breakage due to obstacles [6].

1.2 Aim

This thesis aims to design a multiple-RIS integrated indoor D-MIMO system model operating at 4 GHz frequency (sub-6 GHz range) in the Matlab programming platform. The primary motive is to provide consistent connectivity to the users and to enhance the network parameters of a conventional D-MIMO system. The channel state information (CSI) is assumed to be known to the transmitter to reduce the complexity of problem formulation. An indoor scenario with high obstacle density, such as factories and medical infrastructures, is chosen to address the increased UE demand for synchronous working of the UEs [2]. RISs consisting of passive elements are used to support the low energy consumption aspect of using RISs. The deployment of multiple RISs will concern the population density of UE in the indoor area to maximize the system's service coverage. The parameters of focus include spectral efficiency, energy efficiency, and service coverage probability of the system. The system performance of the RIS-integrated D-MIMO model will be compared with the conventional D-MIMO system model and RIS-integrated MIMO system model to analyze the benefits of deploying RISs in an indoor D-MIMO system for developing an energy-efficient and scalable network for the future.

1.2.1 Limitations

This thesis is bounded by the following limitations:

- Simulations are carried out in this thesis for integrating RISs into the D-MIMO system model to analyze its performance, benefits, and future use cases.

- The D-MIMO system model, which requires channel estimation is not considered in this thesis, as it could make the problem formulation extremely complex.

1.2.2 Specification of the issues being investigated

The problems that are investigated in this thesis include:

- Optimizing RIS phase-shift without introducing significant delay and complexity in the D-MIMO network.
- Network coverage extension limitations during deployment of RISs in an indoor D-MIMO system.
- Influence of RISs on the energy efficiency of the RIS-assisted D-MIMO system.
- Performance parameter optimization of RIS-integrated D-MIMO system.

2
Theory

This section explains the necessary theoretical aspects required to understand the system model's working and interpret the results of its performance parameters. The subsections, including wireless communication, 6G, operational frequency, D-MIMO, RISs, and channel model, are introduced at the beginning to understand the workings of the system model. Later, the subsections, including pathloss, service coverage, spectral efficiency, and energy efficiency, are explained to get a wider view of the system performance and analyze the obtained results.

2.1 Wireless Communication

Due to rapid technological advancement, the number of UEs, IoTs, machines, and other smart devices is growing exponentially. Thus, it is necessary to interconnect these devices with users in an ecosystem to enable users to access their devices at different locations. This leads to the necessity of having wireless channels that allow users to connect with their devices without any physical link. Even though the currently available networks are efficient enough to satisfy user demands, making them energy-efficient is necessary for a sustainable future.
The wireless communication system consists of a transmitter and a receiver unit, which exchange information as signals across a wireless channel. When a signal propagates through such a channel, the additive white Gaussian noise (AWGN) present in the channel alters signal properties like amplitude and phase. Even though this results in obtaining the information with some error at the receiver end, the user can retrieve the data by performing amplitude and phase correction of the signal at the receiver end. For a complex system having multiple obstacles, the data retrieval process becomes highly complex and fails in certain situations. This led to the study of channel estimation to identify the changes a channel introduces in a signal as it propagates. This strategy is used to extract the transmitted information.
The strategy to obtain knowledge about the channel through which we plan to transmit is called channel state information (CSI). It can be performed at the transmitter or receiver end and is termed channel state information at the transmitter (CSIT) and channel state information at the receiver (CSIR), respectively. The former uses pilot transmission from the transmitter to the receiver to obtain channel-induced changes in signal and feedback the CSI back to the transmitter. The latter uses precoding of signal at the transmitter end, which is already known to the receiver, to suppress the channel-induced effect on the transmitted data.
In this thesis, to reduce the problem formulation's complexity and delay in the sys-

tem operation, we assume that CSI is known to the system [3]. An illustration of a wireless communication system is shown in Fig. 2.1.

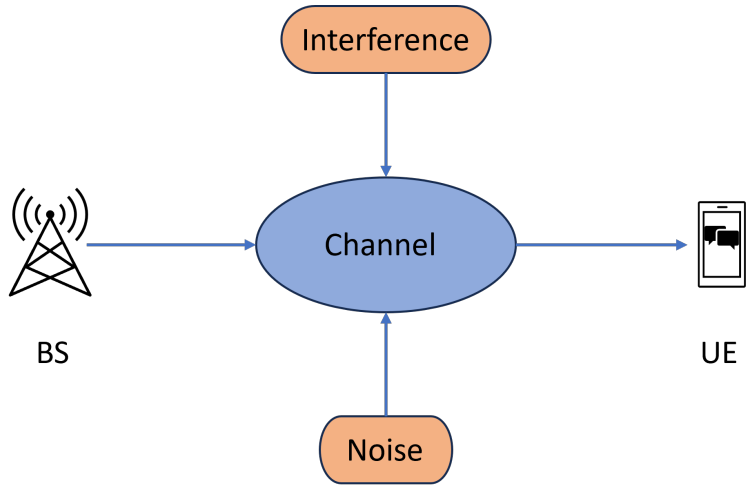

Figure 2.1: Wireless Communication model

2.2 6G

The 6th generation of wireless communication (6G) aims to address user's future demands and add intelligence to wireless networks. 6G mainly focuses on providing higher data rates to users and optimizing parameters, including latency, connectivity, security, spectral efficiency, and energy efficiency. In addition, it also targets adding sensing properties to the network by utilizing high-performance radio units, integrated IoT sensors, and RISs to meet huge user demands in the future.
Unlike its previous generation, 6G aims to connect the users and the physical world. This requires large-scale deployment of sensors and utilization of artificial intelligence (AI) and machine learning (ML) techniques to analyze and interpret the collected data [7]. This helps to create more intelligent and efficient networks for major sectors like telecommunication, transportation, and healthcare.

2.3 Beamforming

The technique used in the latest technologies like LTE and 5G to direct the signal from the transmitter array towards the receiver's exact location in the form of a beam by focusing the signal power is known as beamforming. This technique targets to attain a high signal-to-noise ratio (SNR) at the receiver end. The highly directive nature of the beamforming reduces the chances of a signal undergoing severe path loss while propagating through the channel. When considering a system, this also reduces interference from other sources and enhances the quality of the received signal. The beamforming can be classified into three types based on the strategy used

to steer this signal toward the receiver: analog beamforming, digital beamforming, and hybrid beamforming.

In analog beamforming, the phase shift is introduced to the input signal using a single converter at the point it routes the transmission towards each antenna and is limited to one beam per set of antennas. In the case of digital beamforming, each antenna has its own transceiver and phase converter to operate independently from the rest. Here, it uses a technique called precoding to support multi-stream transmission by integrating and superimposing signals from all the antennas. However, it is not an efficient choice as it utilizes more hardware and requires a lot of signal processing. A hybrid beamforming technique is introduced to tackle these limitations of the above beamforming techniques. Unlike other beamforming strategies, it uses precoding of the input data stream as in digital beamformer and it is routed to each analog beamformer where this data stream is phase-shifted to generate a beam in each analog beamformer [8]. An illustration of an AP transmitting signal toward a UE in a unit cell using beamforming is depicted in Fig. 2.2 below.

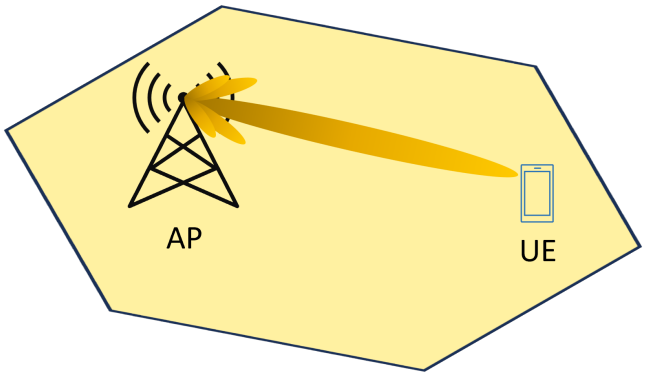

Figure 2.2: Beamforming model

2.4 Operational Frequency

The upcoming 6G network is planned to operate in the mmWave and sub-THz frequency range. In this thesis, 4 GHz frequency in the sub-6 GHz frequency range is used as the carrier frequency (f_c). This is a good choice of carrier frequency as it is very efficient in terms of obstacle penetration compared to higher frequencies, which is a major requirement for a system deployed in an indoor environment. In addition, a system operating at a carrier frequency of 4 GHz suffers less interference compared to common frequency bands such as 2.4 GHz and 5 GHz used for Wi-Fi and Bluetooth.

2.5 D-MIMO

A transmitter-receiver system that uses multiple transmitter and receiver antennas for transmitting and receiving signals between each other is known as a MIMO system. The multiple antennas at the transmitter utilize the beamforming technique, where the signals from all the antennas add constructively to produce a high-power beam that focuses the signal toward the receiver end.
D-MIMO is the latest evolution of the MIMO system, where multiple APs are coordinated and controlled by a core unit. D-MIMO is an efficient method to deploy multiple access points (APs), especially in a high-density macro environment with huge UE connectivity demand. Also, the lower energy consumption and deployment cost make D-MIMO an efficient choice over the MIMO system. Moreover, the scalability property of D-MIMO also makes it a practical option for a large-scale system deployment [1]. An illustration of a D-MIMO system's unit model is depicted in Fig. 2.3 below.

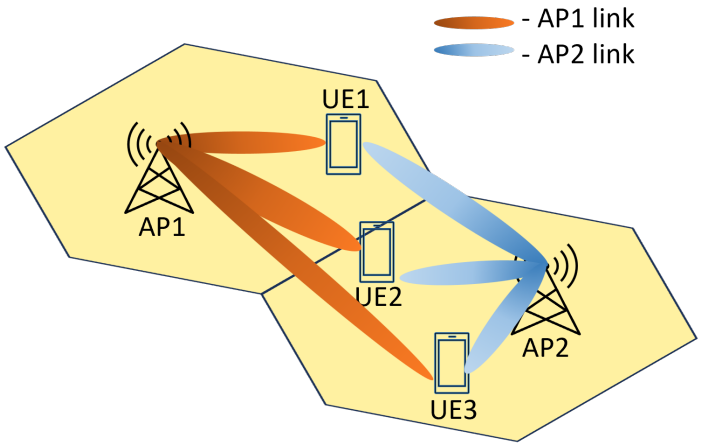

Figure 2.3: D-MIMO unit system

2.6 RIS

A transmitted signal usually fails to reach the receiver end in an environment with high obstacle density. Such scenarios are difficult to avoid even using a multi-AP deployment method like in D-MIMO. The integration of repeaters into such a system helps to resolve this case by redirecting the signals toward the receiver end. However, it is not an effective choice in terms of the system's total energy consumption. Therefore, finding a practical and energy-efficient alternative to resolve this issue is necessary. RIS is the best alternative to the repeaters as it addresses the above-mentioned issue and satisfies the above demands simultaneously. RIS is a planar meshed surface with passive elements occupying each grid that can reconfigure an incident RF signal and redirect it toward any desired receiver. The reconfiguration is done by altering the phase-shift of the RIS elements and then performing beamforming. An illustration of a RIS unit is shown in Fig. 2.4.

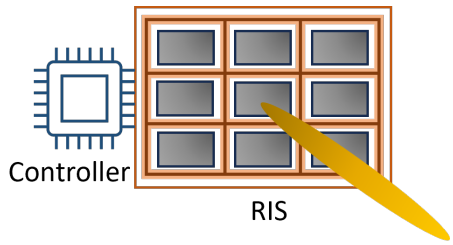

Figure 2.4: RIS unit model

In this thesis, we utilize a RIS constituting of $N \times N$ element, where each element is l-bit reconfigurable to have 2^l combination of amplitude or phase-shifts. Here, a controller is used to alter the phase-shift of the RIS elements to reconfigure an incident signal before reflecting it. The redirecting functionality makes RIS a practical alternative to repeaters, especially in a deployment area with high obstacle density, as depicted in the example scenario in Fig. 2.5.

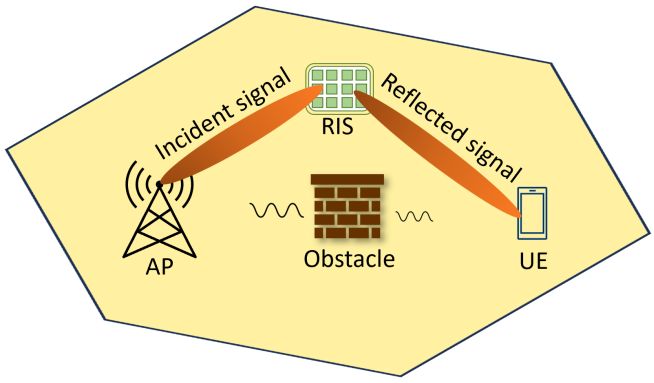

Figure 2.5: RIS working model

The significant advantage of deploying multiple RISs to a network is to attain better service coverage, spectral efficiency, and energy efficiency. RIS's lower energy consumption and passive nature also make it an efficient alternative to a repeater [1]. Other than passive RIS, other models of RIS under research include RIS with a combination of passive, active, and reflecting elements that add intelligence to the RIS. Even though these RIS models enhance the network performance, there will be a trade-off regarding power consumption compared to a passive RIS.

2.7 Channel Model

A channel is a black box with all the information about processes and changes induced to a signal from the point of transmission until it reaches the receiver end.

Therefore, it is crucial to model the channel to study the signal variations and to analyze its influence on the signal properties [9].
The most common way to model a channel is using the matrix method. Here, the channel is modeled in the form of a matrix called a channel matrix. Each element in this matrix is expressed in terms of amplitude and phase, which denotes the gain and phase changes induced by the channel. These changes can be positive or negative depending on the channel properties. Further, the matrix size depends on the number of paths between the transmitting and receiving antennas.

2.8 Pathloss

The magnitude of loss in the power that a transmitted signal suffers along its propagation path is considered as the pathloss of the signal. This parameter is highly dependent on the type of propagation path, obstacle density, the material type of the obstacles, and other environmental factors like rain or snow [10].
This thesis considers an indoor propagation environment for wireless network deployment. Here, a signal is exposed to a lot of power losses due to the high density of stationary and mobile blockages, such as people, walls, furniture, and other equipment, which leads to severe pathloss and shadowing. These losses eventually result in lower coverage for UEs in this environment. The 3rd Generation Partnership Project (3GPP) TR 38.901 indoor hotspot (InH) pathloss model [11] is utilized for measuring these losses in signal power as it closely depicts the influence of indoor channels on a propagating signal.

2.9 Service Coverage

A transmitted signal is supposed to suffer from pathloss as it propagates through a channel. The intensity of the path loss can be influenced by several factors in its propagation path, as mentioned in the above section. In a high pathloss scenario, a transmitted signal might get undetectable by the receiver. It can be either because the received signal strength falls below a particular threshold value of signal strength or the signal fails to reach the receiver.
A user is supposed to be in service coverage if the received power or received data rate satisfies the minimum threshold value for retrieving the transmitted information from the received signal. An indoor environment used here lacks good service coverage due to high blockage density. Thus, it is a significant parameter of concern in a D-MIMO system. Integration of repeaters or RISs is one effective strategy for tackling this problem.
The received data rate (R_u) by a user u can be expressed as below.

$$R_u = B \cdot log_2(1 + \gamma_u), \tag{2.1}$$

Where B denotes the operational bandwidth, and γ_u represents the signal-to-interference-plus-noise ratio (SINR) which is the ratio of the received signal power (P_u) from the serving AP at UE u to the effective noise power and interfering signal power (I_u)

received from other non-serving APs and RISs at UE u.

$$\gamma_u = \frac{P_u}{I_u + \sigma^2}, \tag{2.2}$$

Where σ^2 represents the noise power, which can be expressed as $K \cdot T_0 \cdot B \cdot F_{UE}$, with K the Boltzmann constant ($K \approx 1.38 \times 10^{-23}$J/K), temperature ($T_0$) = 290 K, B the bandwidth of the system in Hz, and F_{UE} the noise figure.
The service coverage probability (χ) is the parameter used for checking whether a user is in coverage of the network or not. By setting a threshold value (R_{th}) for the received data rate (R_u), the availability of service coverage can be categorized [12] as shown below.

$$\chi = \Pr(R_u \geq R_{\text{th}}).$$

2.10 Spectral Efficiency

The parameter used for studying the data transmission rate of a signal transmitted through a channel of a specific bandwidth is known as spectral efficiency (η_{SE}). Recently, the criticality of spectral efficiency has increased drastically due to higher license costs for purchasing spectrum. Thus, it is crucial to utilize the frequency spectrum efficiently using more promising spectrum allocation and utilization strategies. The spectral efficiency of a D-MIMO network can be calculated using the following formula [13].

$$\eta_{SE}(u) = \sum_{u=1}^{N_{UE}} \frac{R_u}{B}, \tag{2.3}$$

Where N_{UE} represents the number of UEs served by the system, and R_u denotes the data rate received by UE u.

2.11 Energy Efficiency

In wireless networks, energy efficiency (η_{EE}) represents whether the energy spent on a network operation is efficiently utilized or not to cut down the energy utilization for the same task by optimizing the way the current network operates.
The energy efficiency of a D-MIMO network is formulated as below.

$$\eta_{EE}(u) = \sum_{U=1}^{N_{UE}} \frac{R_U}{\xi \cdot P_T + P_c}, \tag{2.4}$$

Where N_{UE} denotes the number of UEs served by the system, R_u denotes the data rate received by UE u, ξ represents the inverse of the transmit amplifier efficiency, P_T corresponds to the transmitted power, and P_c denotes to the static power consumption of the whole system [14].

Reducing energy consumption through efficient strategies helps to reduce the consumption of natural resources, promoting sustainability. Due to the above concerns, the environmental damage rate is substantially high, which increases the criticality of energy efficiency parameters while designing and deploying new technologies.

3

Methods

3.1 System model

Two types of system models are analyzed in this thesis. Initially, a conventional indoor D-MIMO system is modeled for a multi-AP serving scenario. At a later stage, multiple RISs are integrated to this D-MIMO system model, and a comparative study of system performance is conducted. A detailed description of the system modeling is discussed below.

3.1.1 Deployment Model

This section describes the modeling strategies used for designing the conventional D-MIMO and RIS-assisted D-MIMO system models. The methods used to deploy APs, RISs, and UE distribution in the system model are discussed below.

3.1.1.1 D-MIMO deployment model for indoor layout

An indoor D-MIMO system is modeled using the 3GPP TR 38.901 indoor hotspot (InH) model for a big hall scenario [11]. An indoor environment of dimension 300 m x 150 m is considered in the InH model. Here, multiple APs with each having N_{TX} antennas and gain G_{TX} are uniformly deployed at a height h_{AP} such the neighboring APs are at the distance of 50 m from each other. The system is chosen to operate at a bandwidth B of 100 MHz with a carrier frequency f_{c} of 4 GHz (sub-6 GHz frequency band). The n UEs each of N_{RX} antennas and gain G_{RX} are randomly distributed in this finite area using finite homogeneous Poisson point process (FHPPP) with a fixed UE density Λ as shown below.

$$\mathrm{Poisson}(\mathrm{N} = n) = \frac{\Lambda^n . e^{-\Lambda}}{n!}, \tag{3.1}$$

The illustration of the simulation model representing a D-MIMO system is shown in Fig. 3.1 and its corresponding unit model is depicted in Fig. 3.2.

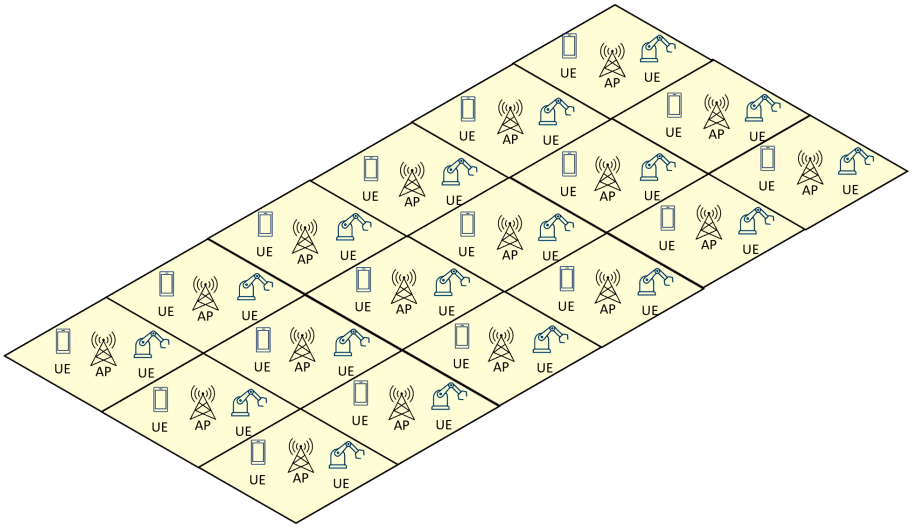

Figure 3.1: D-MIMO system model

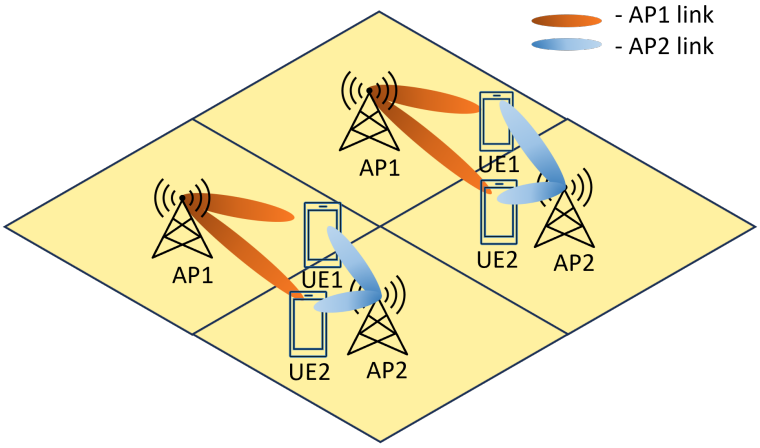

Figure 3.2: D-MIMO system unit model

3.1.1.2 RIS integration in D-MIMO model for indoor layout

RIS is modeled as a meshed square grid model with a total of $N \times N$ elements each of dimensions $\lambda/2 \times \lambda/2$ m^2 and having a gain G_{RIS}. Each RIS element is l-bit reconfigurable and can align towards 2^l combinations of phase shifts to redirect the incident signal to a desired location.
In an indoor environment, a signal transmitted from an AP toward a UE suffers from multiple path loss, resulting in a lack of service coverage. Thus, deploying multiple RISs in such an environment is supposed to resolve this issue. For deploying RISs, the average service coverage probability received by the UEs corresponding to each possible location of 18 RISs with one RIS in each of the 50 m $\times$ 50 m square cell in the deployment area is studied for 500 independent UE realizations. The obtained measurements were ranked to determine the best deployment locations for the 18 RISs that gave the maximum service coverage probability. All 18 RISs are deployed in the overall area, with one RIS each in every cell in a fixed order of the identified

positions. Also, there is a constraint that each RIS in a square cell is in control of the corresponding AP in that square cell. The illustration of the simulation model that represents a RIS-integrated D-MIMO system is shown in Fig. 3.3 and its corresponding unit model is given in Fig. 3.4.

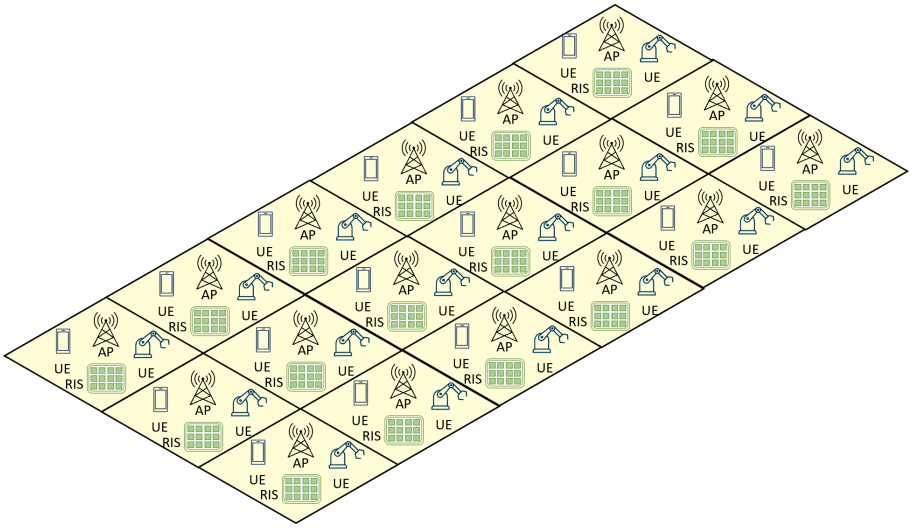

Figure 3.3: RIS integrated D-MIMO system model

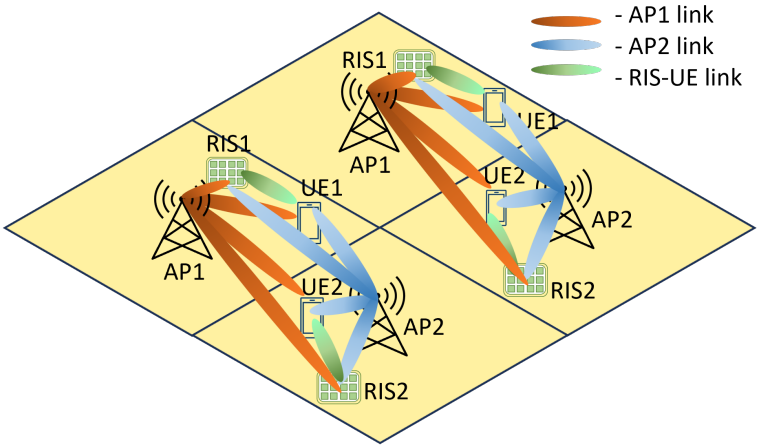

Figure 3.4: RIS integrated D-MIMO system unit model

3.1.2 Channel model

For transmitting a signal from an AP towards a desired UE, the LoS availability is initially checked by using 3GPP TR38.901 line-of-sight (LoS) probability $\mathrm{Pr}_{\mathrm{LoS}}$ model for indoor hotspot (InH) [15]. This model satisfies both the operational frequency range and the indoor scenario. In this model, $\mathrm{Pr}_{\mathrm{LoS}}$ depends on the 2D-Euclidean distance between the serving AP and target UE.

$$\mathrm{Pr}_{\mathrm{LoS}}(d_{\mathrm{2D}}) = \begin{cases} 1, \text{ if } d_{\mathrm{2D}} \leq 1.2 \text{ m}; \\ \exp(\frac{-(d_{\mathrm{2D}}-1.2)}{4.7}), \text{ if } 1.2 \text{ m} < d_{\mathrm{2D}} < 6.5 \text{ m}; \\ \exp(\frac{-(d_{\mathrm{2D}}-6.5)}{32.6}) \cdot 0.32, \text{ if } d_{\mathrm{2D}} \geq 6.5 \text{ m}, \end{cases} \tag{3.2}$$

Where d_{2D} denotes the 2-D Euclidean distance between AP and UE in the horizontal plane in meters.
Once the $\mathrm{Pr}_{\mathrm{LoS}}$ is calculated, a random value is drawn from the range [0,1]. Suppose the obtained value is less than or equal to the obtained $\mathrm{mPr}_{\mathrm{LoS}}$, the LoS link between the AP and UE is categorized as available, or else the LoS link is considered unavailable.
Thus the LoS availability ($\mathrm{A}_{\mathrm{LoS}}$) can formulated as

$$\mathrm{A}_{\mathrm{LoS}}(p) = \begin{cases} 1, & \text{if random}(p) \leq \mathrm{Pr}_{\mathrm{LoS}}, \ \forall \ p \ \epsilon[0,1] \\ 0, & \text{if random}(p) > \mathrm{Pr}_{\mathrm{LoS}}, \ \forall \ p \ \epsilon[0,1]. \end{cases} \tag{3.3}$$

The 3GPP TR 38.901 indoor hotspot (InH) pathloss model [16] is considered for measuring the pathloss between transmitter and receiver. The LoS pathloss ($\delta_{\mathrm{LoS}}(d_{\mathrm{3D}})$) and NLoS pathloss ($\delta_{\mathrm{NLoS}}(d_{\mathrm{3D}})$) are modeled separately w.r.t. the indoor environmental conditions, operational frequency, and the 3D-Euclidean distance d_{3D} between the transmitter and receiver as formulated below.

$$\delta_{\mathrm{LoS}}(d_{\mathrm{3D}}) = 32.4 + 17.3\log_{10}(d_{\mathrm{3D}}) + 20\log_{10}(f_{\mathrm{c}}) + \varepsilon_{\mathrm{LoS}}, \tag{3.4}$$

$$\delta_{\mathrm{NLoS}}(d_{\mathrm{3D}}) = \max(\delta_{\mathrm{LoS}}(d_{\mathrm{3D}}), (38.3\log_{10}(d_{\mathrm{3D}}) + 17.3 + 24.9\log_{10}(f_{\mathrm{c}}))) + \varepsilon_{\mathrm{NLoS}}. \tag{3.5}$$

Where the $\varepsilon_{\mathrm{LoS}}$ and $\varepsilon_{\mathrm{NLoS}}$ represent the shadow fading between the transmitter and receiver in the LoS and NLoS path respectively. The LoS and NLoS shadow fading is modeled as a log-normal distribution with standard deviations $\sigma_{\mathrm{LoS}} = 3$ and $\sigma_{\mathrm{NLoS}} = 8.03$ respectively.

3.1.2.1 Alternating optimization algorithm for joint precoding

An alternating optimization algorithm for joint precoding proposed in [17] is utilized to perform codebook-based beamforming for transmission in the downlink (DL). The above-mentioned algorithm is designed for a narrow-band system and is therefore considered as a foundation to develop a new algorithm to support a wide-band system. The pseudo-code of the algorithm for the wide-band system that is developed is shown in Algorithm 1 and the corresponding 2 APs and 1 RIS coordinately serving a UE scenario is shown in Fig. 3.5. In this algorithm, we assume CSI is already known to the transmitter for analysis purposes.

Algorithm 1 Alternating optimization algorithm-based joint precoding for maximization of received power at UE for a wide-band system

repeat for $\kappa = 1, \ldots, W$ sub-carriers
  Initialize $w[\kappa]$, $q_1[\kappa]$, and $q_2[\kappa]$ to feasible values
  $H_1[\kappa] = \sqrt{\delta(d_{\mathrm{AP_1-RIS}})[\kappa] \cdot G_{\mathrm{TX}} \cdot G_{\mathrm{RIS}}} \cdot H_1^{'}[\kappa]$;
  $H_2[\kappa] = \sqrt{\delta(d_{\mathrm{AP_2-RIS}})[\kappa] \cdot G_{\mathrm{TX}} \cdot G_{\mathrm{RIS}}} \cdot H_2^{'}[\kappa]$;
  $G[\kappa] = \sqrt{\delta(d_{\mathrm{RIS-UE}})[\kappa] \cdot G_{\mathrm{RIS}} \cdot G_{\mathrm{RX}}} \cdot G^{'}[\kappa]$;
  $R_1[\kappa] = \sqrt{\delta(d_{\mathrm{AP_1-UE}})[\kappa] \cdot G_{\mathrm{TX}} \cdot G_{\mathrm{RX}}} \cdot R_1^{'}[\kappa]$;
  $R_2[\kappa] = \sqrt{\delta(d_{\mathrm{AP_2-UE}})[\kappa] \cdot G_{\mathrm{TX}} \cdot G_{\mathrm{RX}}} \cdot R_2^{'}[\kappa]$;
  repeat for n iterations
    $g_w = G[\kappa]^{\mathrm{H}} w[\kappa]$ and $h_q = H_1[\kappa]q_1[\kappa] + H_2[\kappa]q_2[\kappa]$;
    Set $\Phi_n[\kappa] = -\angle g_w(n) h_q(n), \forall$ n $= 1, \ldots,$N;
    Phase correction, $\theta = \angle w[\kappa]^{\mathrm{H}} R_2[\kappa] q_2[\kappa]$;
    $A_1[\kappa] = R_1[\kappa]$; $A_2[\kappa] = (G[\kappa]\Phi[\kappa]H_2[\kappa]e^{-j\theta}) + R_2[\kappa]$;
    $A[\kappa] = A_1[\kappa] + A_2[\kappa]$;
    Perform SVD($A_1[\kappa]$) and SVD($A_2[\kappa]$) to obtain updated $q_1[\kappa]$ and $q_2[\kappa]$ as right unitary matrices;
    Perform SVD($A[\kappa]$) to obtain updated $w[\kappa]$ as left unitary matrix;
  until convergence;
  $P_R[\kappa] =\mid (w[\kappa]^{\mathrm{H}} A_1[\kappa] q_1[\kappa]) + (w[\kappa]^{\mathrm{H}} A_2[\kappa] q_2[\kappa]) \mid^2$
until end;
Perform greedy-algorithm to determine $q_1[\kappa_{opt}]$, $q_2[\kappa_{opt}]$, $w[\kappa_{opt}]$, and $\Phi[\kappa_{opt}]$ corresponding to κ_{opt} which provide $P_R[\kappa]_{max}$;
Utilize $q_1[\kappa_{opt}]$, $q_2[\kappa_{opt}]$, $w[\kappa_{opt}]$, and $\Phi[\kappa_{opt}]$ to re-calculate $P_R[\kappa]$ $\forall$ κ;

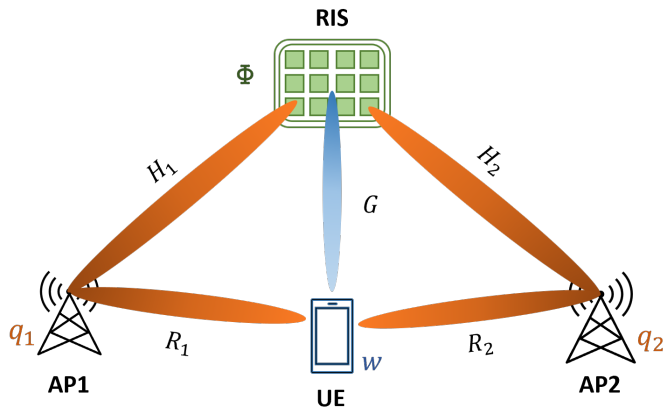

Figure 3.5: Channel model of a single UE serving unit of D-MIMO with 2-AP and 1-RIS serving system.

Here, for simplicity, without the loss of generality, we consider that 2 APs and 1 RIS coordinately serve each UE. The channels $R_1^{'}[\kappa]$ and $R_2^{'}[\kappa]$ represent the channel between $\mathrm{AP_1}$-UE and $\mathrm{AP_2}$-UE respectively corresponding to the sub-carrier κ.

Moreover, the channels $H_1^{'}[\kappa]$, $H_2^{'}[\kappa]$, and $G^{'}[\kappa]$ represent the channel between AP_1-RIS, AP_2-RIS, and RIS-UE respectively corresponding to the sub-carrier κ. Here, the channels are modeled as Rayleigh or Rician channels based on the availability of the LoS. Each channel has its corresponding effect of channel gain and pathloss between the transmitter and receiver. For the Rician channel, the LoS component is influenced by a pair of the array response vector at AP (υ_{TX}), UE (υ_{RX}), or RIS (υ_{RIS}) end. This adds the effect of its respective phase variation to the channel to make it more realistic. The resultant direct channels from both APs are denoted as $R_1[\kappa]$ and $R_2[\kappa]$ and the resultant channel between AP_1-RIS, AP_2-RIS, and RIS-UE are denoted as $H_1[\kappa]$, $H_2[\kappa]$, and $G[\kappa]$ respectively.

The phase-shift matrix of the RIS w.r.t. the sub-carrier κ is represented as $\Phi[\kappa]$. Each $\Phi[\kappa]$ holds the phase shift values $\Phi_{\mathrm{n}}[\kappa]$ for $n = 1, \ldots, N$ on its diagonal, such that $\Phi[\kappa] = \mathrm{diag}(e^{j\Phi_1[\kappa]}, \ldots, e^{j\Phi_N[\kappa]})$. The vectors $q_1[\kappa]$ and $q_2[\kappa]$ are used to represent the unit-norm precoder at AP_1 and AP_2 respectively for the sub-carrier κ. Likewise, $w[\kappa]$ represents the unit-norm combiner at UE w.r.t. the sub-carrier κ. The precoders and combiner are of length N_{TX} and N_{RX} respectively. Here, the precoding and combining channels are denoted as h_q and g_w, respectively.

In this model, the channel from AP_2 is considered to suffer from a high pathloss than from AP_1 based on the AP selection, which is based on pathloss between AP-UE over the sub-carrier κ. Hence, AP_2 requires additional assistance by a RIS, and the RIS's phase-shift should be optimized w.r.t. it and serving UE. Firstly, we initialize $q_1[\kappa]$, $q_2[\kappa]$, and $w[\kappa]$ with feasible values and proceed to maximize $(\mid w[\kappa]^{\mathrm{H}} G[\kappa]\Phi[\kappa]H_2[\kappa]q_2[\kappa] \mid^2)$ and $(\mid w[\kappa]^{\mathrm{H}} R_1[\kappa]q_1[\kappa] \mid^2 + \mid w[\kappa]^{\mathrm{H}} R_2[\kappa]q_2[\kappa] \mid^2)$ by alternatively optimizing $\Phi[\kappa]$. Later, repeat the same process vice-versa by fixing this obtained value of $\Phi[\kappa]$ and optimize $q_1[\kappa]$, $q_2[\kappa]$, and $w[\kappa]$. Here, singular value decomposition (SVD) is applied to the combined channel consisting of the direct channel and the channel via RIS to extract the unitary matrix representing the $q_1[\kappa]$, $q_2[\kappa]$, and $w[\kappa]$ at each step. The process is repeated for multiple iterations until convergence of the objective function.

The received signals by UE through both the direct path from both the APs and the path via RIS gets coherently combined at the UE to obtain the signal power as $\mid w[\kappa]^{\mathrm{H}} G[\kappa]\Phi[\kappa]H_1[\kappa]q_1[\kappa] + w[\kappa]^{\mathrm{H}} R_1[\kappa]q_1[\kappa] + w[\kappa]^{\mathrm{H}} G[\kappa]\Phi[\kappa]H_2[\kappa]q_2[\kappa] + w[\kappa]^{\mathrm{H}} R_2[\kappa]q_2[\kappa] \mid^2$. This process is repeated for all the W sub-carriers, and its corresponding received power at target UE $P_R[\kappa]$ is computed. Utilizing this $P_R[\kappa]$, we perform greedy-algorithm to determine the sub-carrier κ_{opt} that provides the maximum received power $P_R[\kappa]_{max}$. Afterwards, the $q_1[\kappa_{opt}]$, $q_2[\kappa_{opt}]$, $w[\kappa_{opt}]$, and $\Phi[\kappa_{opt}]$ corresponding to κ_{opt} are used to re-calculate the $P_R[\kappa]$ values.

In this thesis, we assume that the channel is the same for all the sub-carriers of the wide-band channel because there will be only negligible variation among the sub-carriers of a wide-band channel. This same algorithm can be scaled for a larger serving AP cluster size ζ_{AP} by combining the channels from each AP while alternatively optimizing its corresponding values of q, w, and Φ.

3.1.2.2 AP-RIS-UE association and scheduling model

It is crucial to create an association-strategy-based model for efficient working of the system model. Here, we use the uniform clustering scheme (UCS) [18] to allocate the available resources uniformly among all the APs present in the system. Furthermore, we use a queue-based scheduling scheme (QSS) [18], responsible for assigning the APs and RISs for serving UEs in a particular timeslot t. This selection process is done by assigning an availability status to each AP and RIS based on the maximum possible UEs it can simultaneously serve.

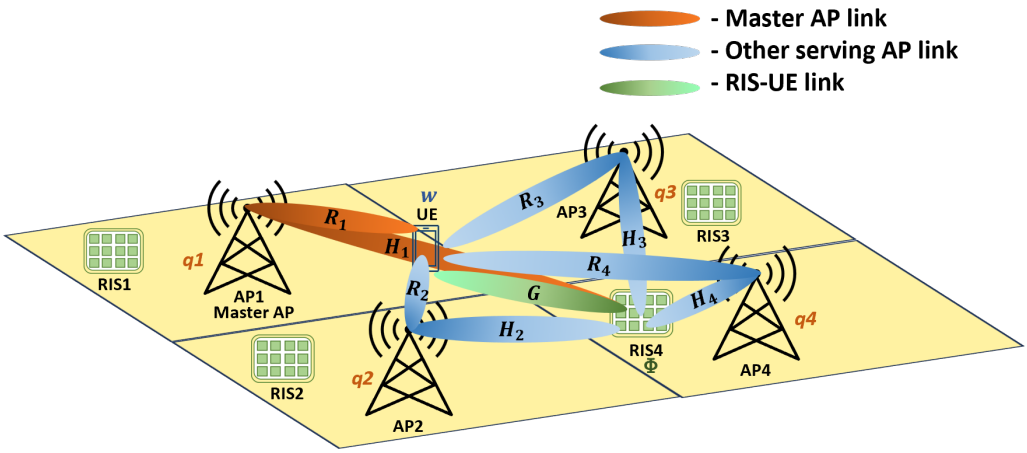

Figure 3.6: RIS integrated D-MIMO system unit model representing a 4 AP cluster and 1 RIS serving an UE scenarios.

The QSS utilizes a UE-centric AP clustering approach as proposed in [18]. A UE initially selects a master AP with the least path loss from the available APs. This master AP checks if the number of available APs and RISs in a particular timeslot satifys the minimum number of APs and RISs required to serve an UE. If this condition is satisfied, the master AP selects the number of serving APs (p) with the best channel condition from the available APs and the serving RISs (s) corresponding to the AP with the worst channel between the serving UE from the selected APs, for coordinately serving the UE.
Additionally, a distance constraint is also added for AP cluster selection to prevent the selection of faraway APs, as those APs cannot serve the UEs efficiently. The unit model of RIS-integrated D-MIMO system with 4 APs and 1 RIS serving a UE scenario is illustrated in Fig. 3.6. This selection of APs and RISs by UE makes the selection process UE-centric, other than having a predefined serving APs and RISs based on the coverage area. If the master AP couldn't find the minimum required APs and RISs to serve the UE, this UE gets served in a later time slot. This strategic serving of UEs ensures that, in the end, all the k UEs in the system are served fairly.

3.1.2.3 Uniform Power Allocation model

In this system, a uniform power allocation strategy is used to assign the transmit power $P_{\mathrm{T}}(n, k)$ to n APs for serving its corresponding UE k. The objective of this

strategy is to uniformly allocate a fixed transmit power of each AP to its corresponding transmitter antennas. This equal power allocation helps to serve each UE k fairly and simplifies the transmit power distribution.

3.1.3 Measurement method

This section describes the measurement of parameters like received power at UE, interference at UE, and system performance metrics such as SINR (γ), data rate (R), service coverage probability (χ), spectral efficiency (η_{SE}), and energy efficiency (η_{EE}) in detail.

3.1.3.1 Received power and interference measurement

The system operates in a way that each UE to be served receives the signal from its serving AP cluster and RISs of size S_{AP} and S_{RIS} respectively based on its availability in a time slot. The signals from the serving APs and the ones through the serving RISs get coherently combined at the UE to form the received signal power. The reflections from other non-serving APs and configured RISs in the system of size I_{AP} and I_{RIS} respectively get additively combined to form the total interference at the serving UE. The received signal power P_k at the UE k that is being served can be expressed as.

$$P_k = \sqrt{P_{\mathrm{T}}} \mid \sum_{n=1}^{S_{\mathrm{AP}}} \sum_{r=1}^{S_{\mathrm{RIS}}} P_{\mathrm{RX}}(k,n,r) \mid^2, \tag{3.6}$$

where,

$$P_{\mathrm{RX}}(k,n,r) = w_k^{\mathrm{H}}(R_{n,k} + (G_{r,k}.\Phi_r.H_{n,r}))q_n, \tag{3.7}$$

The total interference signal I_k at the UE k from the non-serving APs and RISs can be expressed as.

$$I_k = \sqrt{P_{\mathrm{T}}} \mid \sum_{n'=1}^{I_{\mathrm{AP}}} \sum_{r'=1}^{I_{\mathrm{RIS}}} P_{\mathrm{RX}}(k,n',r') \mid^2, \tag{3.8}$$

where,

$$P_{\mathrm{RX}}(k,n',r') = w_k^{\mathrm{H}}(R_{n',k} + (G_{r',k}.\Phi_{r'}.H_{n',r'}))q_{n'}, \tag{3.9}$$

3.1.3.2 Signal-to-Interference-plus-Noise ratio (SINR) measurement

The SINR γ_{k} observed at UE k measures the strength of the desired signal power received P_k w.r.t. the effective interference I_k and AWGN noise power σ_{k}^2 at UE k as shown below.

$$\gamma_{\mathrm{k}} = \frac{P_k}{I_k + \sigma_k^2}, \tag{3.10}$$

3.1.3.3 Data rate measurement

The data rate R_k received by the UE k can be measured using the Shannon-Hartley theorem, which gives the upper bound of the rate of transmission of information through a channel for a defined bandwidth B in the presence of noise as stated below.

$$R_k = B \cdot \log_2(1 + \gamma_k). \tag{3.11}$$

3.1.3.4 Service coverage probability measurement

Service coverage probability χ_{k} of UE k is used to validate whether the received data rate (R_k) satisfies the minimum reliable threshold data rate (R_{th}) or not to consider the UE to be in the service coverage as shown below.

$$\chi_{\mathrm{k}} = \begin{cases} 1, & \text{if } R_k \geq R_{th} \\ 0, & \text{if } R_k < R_{th}. \end{cases} \tag{3.12}$$

3.1.3.5 Spectral efficiency and energy efficiency measurement

Spectral efficiency (η_{SE}) is used to calculate the maximum data throughput over a given bandwidth B. Whereas energy efficiency (η_{EE}) measures the rate at which data can be sent over a unit of power consumption. The spectral efficiency $\eta_{\mathrm{SE}}(k)$ [13] and energy efficiency $\eta_{\mathrm{EE}}(k)$ [14] while serving UE k can be formulated as below.

$$\eta_{\mathrm{SE}}(k) = \frac{R_k}{B}, \tag{3.13}$$

$$\eta_{\mathrm{EE}}(k) = \frac{R_k}{\xi P_{\mathrm{T}} + P_{\mathrm{c}}}, \tag{3.14}$$

Where ξ represents the inverse of the transmit amplifier efficiency (at ideal state, efficiency is equal to 1), the P_{T} and P_{c} represent the transmit power (in Watt) and static power consumption of the whole system (in Watt) respectively.

The static power consumption P_{c} of the whole system [14] is modeled based on the static power consumption $P_{\mathrm{AP_{static}}}$ at AP, $P_{\mathrm{UE_{static}}}$ at UE, P_{b} at each RIS element, and P_{CB} [19] at RIS controller board as shown below.

$$P_{\mathrm{c}} = P_{\mathrm{AP_{static}}} + P_{\mathrm{UE_{static}}} + (N_{\mathrm{RIS}}.P_{\mathrm{b}}) + P_{\mathrm{CB}}. \tag{3.15}$$

Where N_{RIS} is the number of RIS elements at RIS, and all values are in linear units (Watt).
The same procedure is repeated for all UEs, and their corresponding data rate, service coverage probability, spectral efficiency, and energy efficiency are calculated. Their average value gives the overall system performance.

4

Results and discussions

The simulations are carried out for both conventional D-MIMO indoor system models as well as for RIS-assisted D-MIMO indoor system models for comparative study and to analyze the benefits and use cases of deploying RISs in a D-MIMO network. The 3GPP TR 38.901 big hall model is used for indoor modeling and AP deployment. Both the Rayleigh and Rician channel models are considered for channel modeling. The system parameters used for the setup are given in [Table 4.1] below,

Table 4.1: System parameters

Parameters	**Value**
Carrier frequency (f_c)	4 GHz
Operational bandwidth (B) and number of sub-carriers (κ)	100 MHz and 10
Dimension of indoor layout	300 m x 150 m
Dimension of square grid	50 m x 50 m
Number of APs (N_{AP})	18
Number of UEs (N_{UE})	100
Number of transmit antennas(N_{AP})	4
Number of receiver antennas(N_{UE})	1
Height of AP (h_{AP})	2.5 m
Average UE height (h_{UE})	1.5 m
Total transmit power (P_{T})	25 dBm
Noise figure (F_{UE})	10 dB
Pathloss exponent for LoS and NLoS	3 and 8.03
Dimension of an RIS element	$\lambda/2$ x $\lambda/2$
Height of RIS (h_{RIS})	2 m
Number of RIS elements (N_{RIS})	128
Gain of the transmit antenna (G_{TX})	5 dB
Gain of the receiver antenna (G_{RX})	2 dB
Gain of a RIS element (G_{RIS})	4 dB
Threshold data rate (R_{th})	100 Mbps
Static power dissipation at AP ($P_{\mathrm{AP}_{\mathrm{static}}}$)	9 dBW
Static power dissipation at UE ($P_{\mathrm{UE}_{\mathrm{static}}}$)	10 dBm
Static power dissipation at a RIS element (P_{b})	0.01 dBm
Static power dissipation at the RIS controller board (P_{CB})	4.8 W

4.1 Deployment Models

In this section, we discuss the deployment models used for the comparative study of the conventional D-MIMO system model and RIS-integrated D-MIMO system model. The rectangular deployment area of dimensions 300 m x 150 m is used to depict the indoor model. The entire area is divided into a mesh of 6 x 3 square grids with each dimensioned 50 m x 50 m.

4.1.1 D-MIMO system model

In the DMIMO model, the 18 APs are uniformly deployed in the total deployment area. The 100 UEs are randomly deployed in the entire area using a finite homogeneous Poisson point process (FHPPP) and these locations of UEs are fixed during the analysis for the comparative study purpose. The deployment model of the D-MIMO system is represented in Fig. 4.1. As discussed in the system model, each UE is served by an AP cluster based on the availability, pathloss, and distance constraints such that the serving APs are capable of enhancing the received signal strength at the served UE.

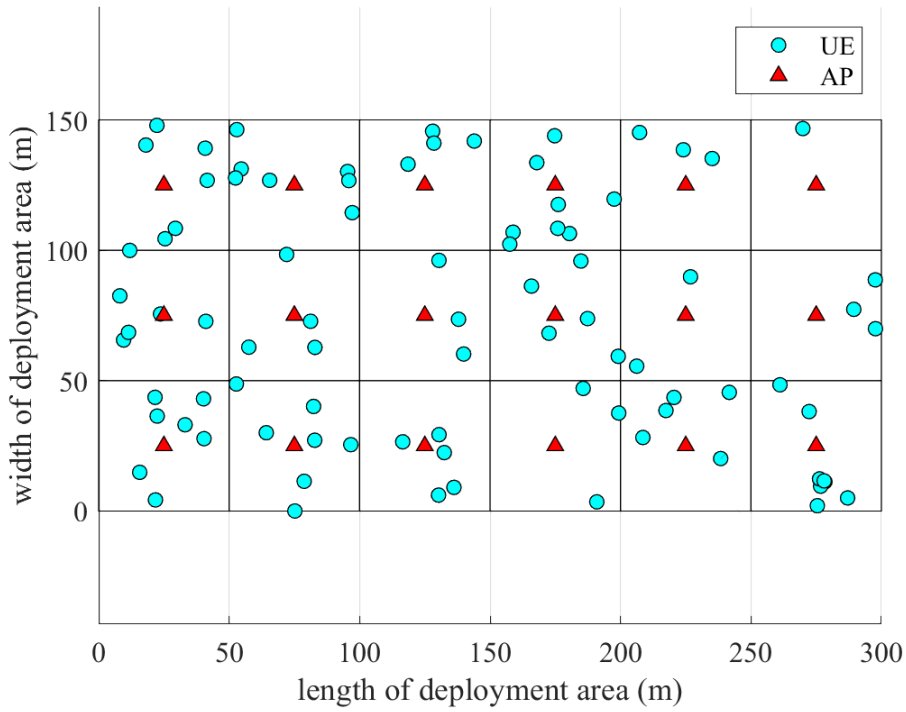

Figure 4.1: Deployment model of D-MIMO system.

4.1.2 RIS-assisted D-MIMO system model

In this model, in addition to the APs in the conventional D-MIMO model, RISs are also deployed to assist the APs in coordinately serving the UEs. To deploy the RISs, the service coverage probability is studied for different locations of RISs in

the entire deployment area for 500 independent realizations of UEs. Utilizing these measured values, the locations that gave maximum service coverage probability for the whole system are identified. These identified best locations of RISs are used to deploy 18 RISs in a fixed pattern. In addition, there is a condition that each RIS in a square grid is in the control of the corresponding AP in that square grid. Unlike in the conventional D-MIMO system model, each UE is served by an AP cluster and an RIS that supports the AP with the weakest channel towards the UE among its serving AP cluster. Like the AP cluster selection process in the conventional D-MIMO system, the RIS selection process is also based on the availability of RISs. The deployment model of the RIS-integrated D-MIMO system is depicted in Fig. 4.2.

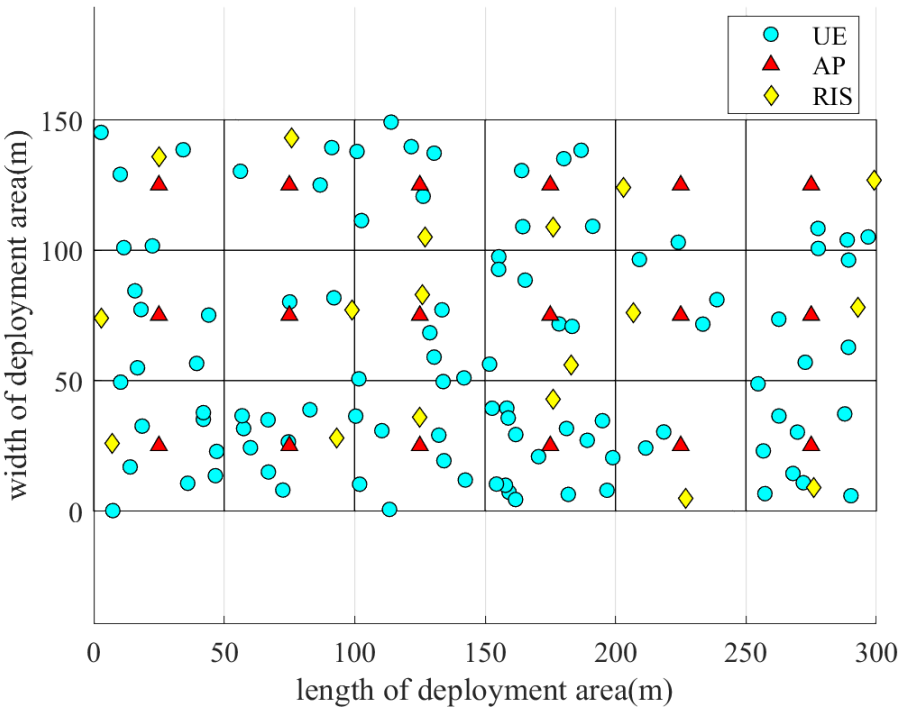

Figure 4.2: Deployment model of RIS-assisted D-MIMO system.

4.2 Performance analysis

The analysis process can be classified into four stages which includes: a) Perform CDF (cumulative distribution function) comparison of SINR at UEs for the conventional D-MIMO system corresponding to different AP cluster sizes to determine the optimal ζ_{AP} value for which the system provides the best performance in terms of SINR γ at UEs, b) Utilize this identified best three ζ_{AP} values, compare the CDF of SINR at UEs for the D-MIMO system models with and without RIS integration in order to determine whether deploying RISs is able to create a significant performance improvement to the conventional D-MIMO system, c) Analyze the CDF of SINR at UEs in the RIS-assisted D-MIMO system corresponding to the best three ζ_{AP} values for two different transmit power at APs (P_{T}) for studying the influence

of (P_{T}) over the SINR at UEs, and d) and e) Analyses the performance parameters, energy efficiency η_{EE} and service coverage probability χ of the RIS-integrated D-MIMO system by varying the N_{RIS} over a large range to investigate the impact of RIS size on these KPIs.

4.2.1 Analysis of optimal AP cluster size for D-MIMO system

The SINR of UEs in the D-MIMO system is analyzed over a range of ζ_{AP} values from 1 to 6 to determine optimal ζ_{AP} values. Here, the ζ_{AP} values from 2 to 6 depict the D-MIMO system whereas, $\zeta_{\mathrm{AP}} = 1$ represents the MIMO system. The corresponding SINR plots are illustrated in Fig. 4.3. Also, the median SINR (γ_{median}) values corresponding to different ζ_{AP} of the D-MIMO system model are given in Table 4.2.

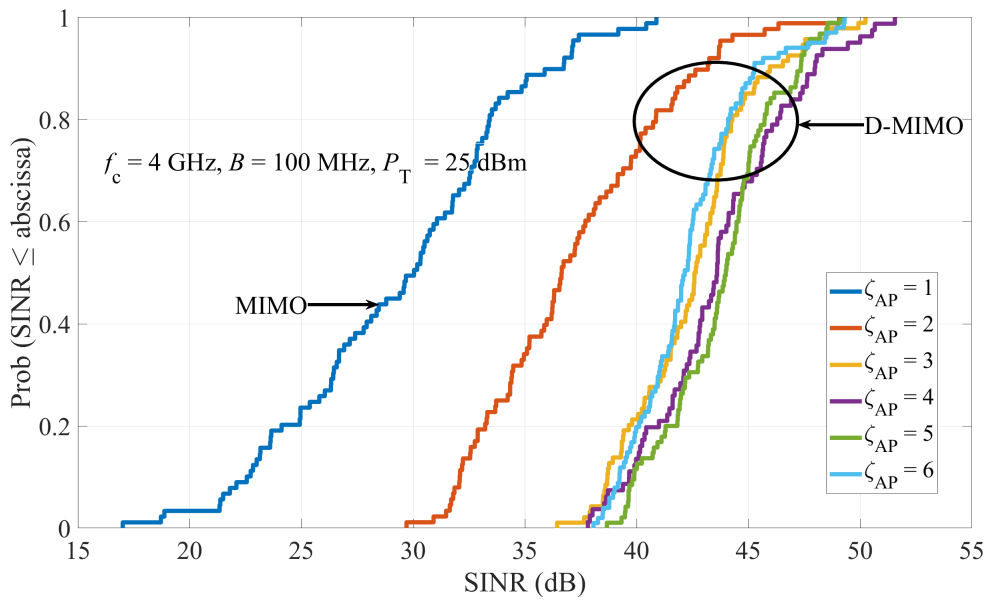

Figure 4.3: SINR CDF comparison between conventional D-MIMO system with different AP cluster sizes i) 1, ii) 2, iii) 3, iv) 4, v) 5, and vi) 6 with $f_{\mathrm{c}} = 4$ GHz, $B = 100$ MHz, and $P_{\mathrm{T}} = 25$ dBm.

Table 4.2: Median SINR of UEs analysis w.r.t. AP cluster size.

ζ_{AP}	1	2	3	4	5	6
γ_{median} **of UEs (dB)**	32.04	36.65	42.65	43.60	44.02	42.29

From Table 4.2, it can be observed that the γ_{median} of UEs in the system show a consistent trend as we scaled the ζ_{AP} value from 1 to 3 because the received power at served UEs are dominant in comparison to the effective total interference and noise power at the served UEs. For larger value of ζ_{AP}, only a slight increase in γ_{median} of UEs are visible as we moved from $\zeta_{\mathrm{AP}} = 3$ to $\zeta_{\mathrm{AP}} = 4$. The increasing rate

is dropping from $\zeta_{\mathrm{AP}} = 3$ to $\zeta_{\mathrm{AP}} = 5$ since the received power at the served UEs is only just enough to balance the resultant interference power and noise power at the served UEs. Whereas at $\zeta_{\mathrm{AP}} = 6$, the γ_{median} value dropped drastically such that it was lower than that of $\zeta_{\mathrm{AP}} = 3$. This drop is due to the dominance of overall interference and noise power at the served UEs compared to the received power at served UEs, which shows the insignificance of increasing ζ_{AP} after a certain threshold value. Likewise, this trend is supposed to continue if we increase the ζ_{AP} further.
From the above graph, it can be seen that the D-MIMO system model outperforms the MIMO system model in terms of SINR for all the ζ_{AP} values from 2 to 6 but with major enhancement observed at $\zeta_{\mathrm{AP}} = 2$ and $\zeta_{\mathrm{AP}} = 3$. Therefore, from the above results, we can conclude that ζ_{AP} 2 and 3 are the best choices of ζ_{AP} for the conventional D-MIMO system over the considered ζ_{AP} range.

4.2.2 Enhancement in D-MIMO performance with RIS integration w.r.t. different AP cluster sizes

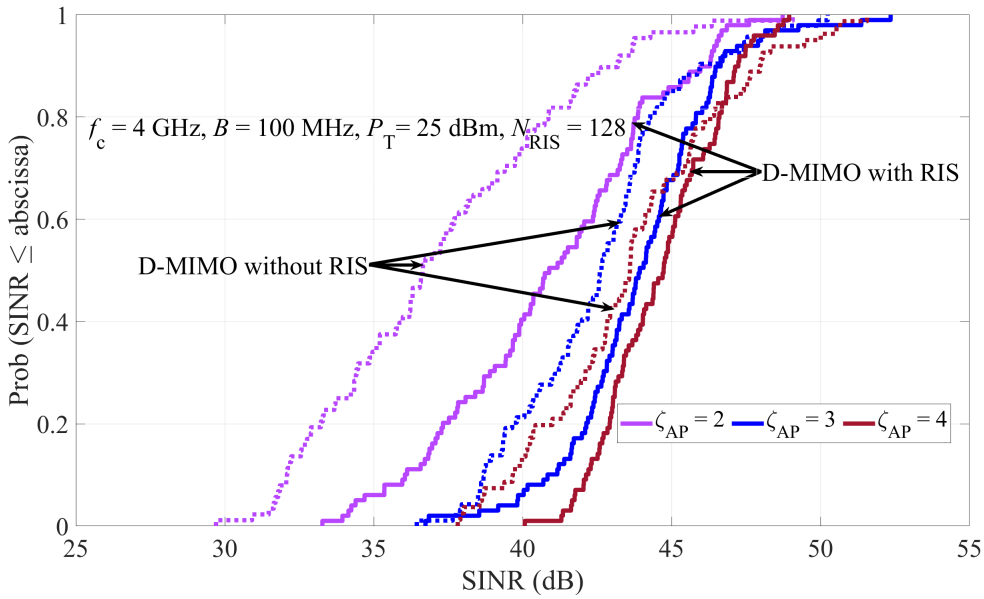

Figure 4.4: SINR CDF comparison between D-MIMO system with and without RIS for different AP cluster sizes i) 2 AP, ii) 3 AP, and iii) 4 AP with $f_{\mathrm{c}} = 4$ GHz, $B = 100$ MHz, and $P_{\mathrm{T}} = 25$ dBm.

In this analysis, we perform a comparative study of SINR at the served UEs between the conventional D-MIMO system model and the RIS-assisted D-MIMO system model to investigate if a RIS-assisted D-MIMO system is able to outperform a traditional D-MIMO's system performance in terms of SINR. This study also examines the significance of integrating RIS to the system. The D-MIMO system is analyzed for the best three ζ_{AP} values i) 2, ii) 3, and iii) 4 obtained in the previous section. In addition to the AP cluster, we use 1 RIS with $N_{\mathrm{RIS}} = 128$ for coordinately serving each UE. Here, the phase-shift of the RIS is optimized to support the AP with the highest pathloss among the serving AP cluster corresponding to

each UE. The SINR CDF at the UEs in the above system models were analyzed and compared with the SINR CDF at the UEs for the conventional D-MIMO system with the same ζ_{AP}. The comparative analysis results are shown in Fig. 4.4.
Furthermore, the additional coordination with a single RIS in serving each UE made a significant improvement of γ_{median} by $\approx$ 4.5 dB, $\approx$ 1.3 dB, and $\approx$ 1.1 dB corresponding to $\zeta_{\mathrm{AP}} = 2$, $\zeta_{\mathrm{AP}} = 3$, and $\zeta_{\mathrm{AP}} = 4$ respectively. The enhancement in γ_{median} were substantially notable in the case of $\zeta_{\mathrm{AP}} = 2$ in comparison to $\zeta_{\mathrm{AP}} = 3$ and $\zeta_{\mathrm{AP}} = 4$. Even though the γ_{median} improvement was smaller for ζ_{AP} values 3 and 4, the impact of RIS is still visible. A declining trend was observed in the enhancement rate with the integration of RISs as we increase ζ_{AP}. Even though RISs assist the AP clusters in serving UEs by creating an additional serving link, the interference from other non-serving APs also gets reflected by this RIS and other RISs pointing towards the direction of the serving UEs. This negative impact of RIS is smaller for lower ζ_{AP} values like two but more visible as we increase ζ_{AP}.
It can also be noticed that the γ_{median} corresponding to $\zeta_{\mathrm{AP}} = 3$ for the RIS-assisted D-MIMO system outperforms the conventional D-MIMO system with $\zeta_{\mathrm{AP}} = 4$. Here, it shows the potential of RIS in replacing a traditional D-MIMO system with a larger ζ_{AP} by a RIS-integrated D-MIMO system with a comparatively smaller ζ_{AP} value. From the above observations, it is clear that the SINR improvement is more visible with RIS integration, especially for smaller ζ_{AP} values like 2. The above analysis also shows that the potential of a RIS-assisted D-MIMO system with $\zeta_{\mathrm{AP}} = 3$ to replace a conventional D-MIMO system with a larger ζ_{AP} of 4. The above results prove the SINR enhancement capability of the RIS when deployed in a regular D-MIMO system.

4.2.3 Performance analysis of different AP cluster sizes w.r.t. transmit power of AP for RIS-assisted D-MIMO system

In this section, we analyze the SINR CDF at the UEs for different ζ_{AP} values including, i) 2, ii) 3, and iii) 4 for the RIS-integrated D-MIMO system model corresponding to two different transmit power values of AP, $P_{\mathrm{T}} = 25$ dBm and $P_{\mathrm{T}} = 30$ dBm. This analysis is performed to study the influence of transmit power at AP on the SINR at UEs in an RIS-assisted D-MIMO system. The results corresponding to the above scenarios are shown in Fig. 4.5.
It can be observed that, when the P_{T} was increased by 5 dBm, there was a significant rise in γ_{median} by 4 dB, 3.5 dB, and 5 dB corresponding to ζ_{AP} values 2, 3, and 4 respectively. This shows the influence of P_{T} in improving the SINR at UEs. Furthermore, a consistent performance improvement was observed for all three cases of the system model when we increased the P_{T} value. This consistency was found lacking for the scenario with $P_{\mathrm{T}} = 25$ dBm.
It can also be noticed that the rise in P_{T} corresponding to case i) was able to outperform case iii) with $P_{\mathrm{T}} = 25$ dBm. This shows the potential of P_{T} in replacing a RIS-assisted D-MIMO system with a larger ζ_{AP} by a similar system of smaller ζ_{AP} and an increased P_{T}. Even though this is a potential strategy, there is always a trade-off between the SINR and energy consumption when considering the overall

system. This trade-off might be less visible for a small-scale indoor D-MIMO system, but it can be huge for a D-MIMO system deployed on a large-scale.

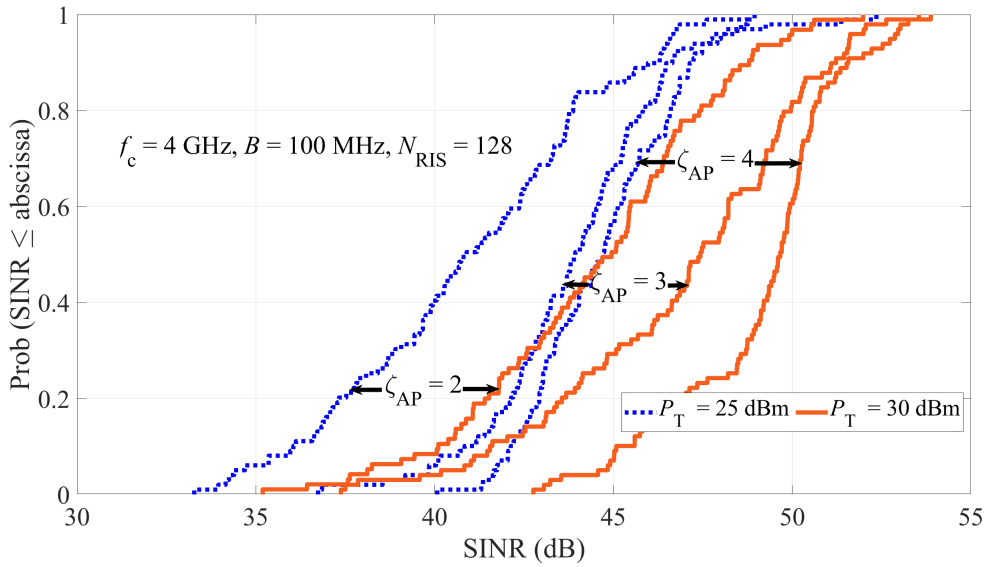

Figure 4.5: SINR cdf comparison between to different AP cluster sizes for transmit powers i) P_T = 25 dBm, and ii) P_T = 30 dBm with f_c = 4 GHz, B = 100 MHz, N_{RIS} = 128, and G_{RIS} = 4 dB.

4.2.4 Energy efficiency analysis of RIS-integrated D-MIMO system

In this analysis, the average energy efficiency η_{EE} of the RIS-integrated MIMO (scenario a) $\zeta_{AP} = 1$) and D-MIMO (scenario b) $\zeta_{AP} = 2$ and scenario c) $\zeta_{AP} = 3$) systems were analyzed by varying the N_{RIS} over a range of 1 to 256 to study its influence over η_{EE}. Other than transmit power, the static power consumption of AP, UE, RIS element (in Pin-diode model), and RIS control board were also considered while measuring η_{EE} of the system model. This analysis is performed for three static power consumption values of RIS element (P_b) which include i) 0.01 dBm corresponding to the ideal passive RIS element and ii) 5 dBm and iii) 10 dBm corresponding to a practical passive RIS element. The results for the above 3 cases corresponding to both RIS-integrated MIMO and D-MIMO systems are shown in Fig. 4.6.

The energy efficiency of the conventional MIMO system with $\zeta_{AP} = 1$ and D-MIMO system with ζ_{AP} values 2 and 3 were measured to be 8.06 Mbps/J, 10.01 Mbps/J, and 10.65 Mbps/J respectively. With the integration of RIS to these systems, the corresponding energy efficiency values are observed to be improved. In case of scenarios a) and b), it can be noticed that the η_{EE} values show an increasing trend over the considered N_{RIS} range for case i) of P_b. Even though the η_{EE} values are found to be increasing for case i) as we moved over the considered N_{RIS} range for all the scenarios, the increasing rate is dropping drastically as we moved from scenario a) to c). This trend is because the increase in received data rate at UEs in scenario a) was dominant to the system's overall power consumption as we increase the N_{RIS}.

However, in the case of scenario c) with case i), the received data rate at UEs was just enough to compensate for the system's total power consumption in a multi-AP serving scenario. This resulted in having only similar improvement in η_{EE} over the N_{RIS} range for the above case. Even though the η_{EE} values show an increasing trend for case ii) in scenario a), it was observed to be declining for scenario b) and c).

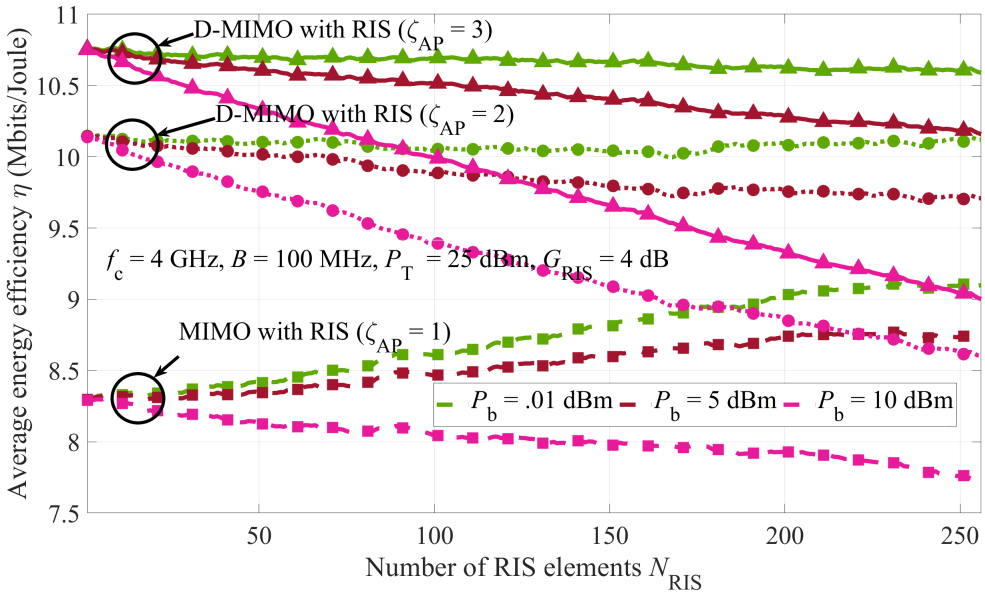

Figure 4.6: Energy efficiency analysis w.r.t. the number of RIS elements for RIS-integrated MIMO and D-MIMO models with $f_{\mathrm{c}} = 4$ GHz, $B = 100$ MHz, $P_{\mathrm{T}} = 25$ dBm, and $G_{\mathrm{RIS}} = 4$ dB.

For case iii), all the scenarios show a declining trend, with the dropping rate increasing as we move from scenario a) to c). However, when we check the η_{EE} values corresponding to the initial count of N_{RIS}, we can observe a good improvement of 1.85 Mbits/J between scenario a) and b) but this gap gets reduced to 0.62 as we increase the ζ_{AP} moving from scenario b) to c). Even though the drop rate of η_{EE} for case iii) of the D-MIMO system is huge, the values obtained are still better than that for case i) of the MIMO system until N_{RIS} value of ≈ 170 and ≈ 230 for the scenarios b) and c) respectively. The obtained results show the advantage of a D-MIMO system over a MIMO system and the potential of integrating RISs with passive elements to these systems in enhancing η_{EE}.

4.2.5 Service coverage probability analysis of RIS-assisted D-MIMO system

In this analysis, the service coverage probability χ is analyzed for both RIS-integrated MIMO and D-MIMO systems w.r.t. N_{RIS} to study its influence on χ. The D-MIMO system is analyzed for two cases, i) $\zeta_{\mathrm{AP}} = 2$ and ii) $\zeta_{\mathrm{AP}} = 3$. The analysis results for the systems are shown in Fig. 4.7.

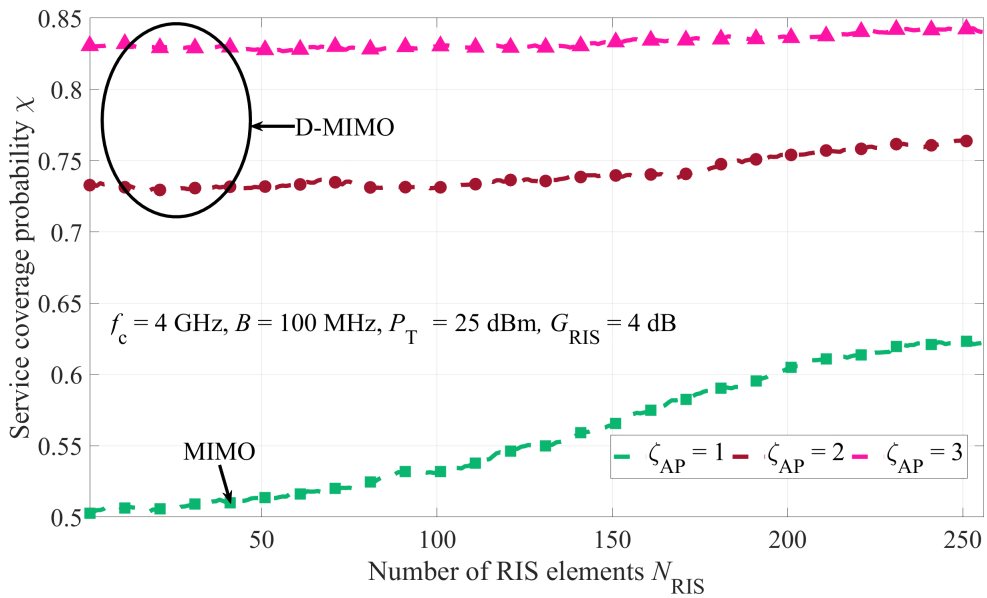

Figure 4.7: Service coverage probability analysis w.r.t. the number of RIS elements for MIMO and D-MIMO models with $f_c = 4$ GHz, $B = 100$ MHz, $P_T = 25$ dBm, and $G_{RIS} = 4$ dB.

From this graph, it can be observed that there is a rise in χ in both MIMO and D-MIMO systems as we vary N_{RIS} over the range from 1 to 256. The increasing rate of χ for the D-MIMO system was slow with an improvement of $\approx 3\%$ and $\approx 1\%$ between the least and maximum value of the considered N_{RIS} range corresponding to case i) and ii) respectively. However, the improvement rate of χ was significantly large for the MIMO system compared to the D-MIMO system with an enhancement gap of $\approx 12\%$. Even though the enhancement gap of χ in the D-MIMO system corresponding to case i) was less compared to the MIMO system, the service coverage in this D-MIMO system was $\approx 23\%$ and $\approx 14\%$ higher than that of MIMO system at the lowest and highest value of the considered N_{RIS} range. These results show the advantage of using the D-MIMO system over the MIMO system in terms of service coverage due to the multi-AP serving scenario present in the D-MIMO system. Furthermore, the service coverage probability improved further as the N_{RIS} of the supporting RISs is increased.

It can be noticed that the D-MIMO system corresponding to case ii) shows an additional enhancement of $\approx 10\%$ and $\approx 8\%$ at the least and most N_{RIS} values when compared to the D-MIMO system with case i). This notable improvement in χ is obtained due to an additional serving AP in the D-MIMO system with case ii) compared to the D-MIMO system with case i). These results show that the D-MIMO system outperforms the MIMO system in terms of service coverage. Furthermore, additional enhancement in service coverage can be introduced to the system with the integration of RISs to serve the UEs in the system. Also, this enhancement gets increased further as we increase the N_{RIS} of each serving RIS in an RIS-assisted D-MIMO system.

5
Conclusions

In this thesis, we performed a comparative study of an indoor conventional D-MIMO system model and an indoor RIS-assisted D-MIMO system model with high UE density to study the performance improvement of the system with the integration of RIS. A uniform cluster scheme is used to jointly serve UEs using multiple APs. An alternating optimization algorithm was adopted for the joint precoding for this multi-AP serving scenario. Fair scheduling and queue-based approaches were used to efficiently serve the UEs in the system. Different AP cluster sizes were considered for serving the UEs in a D-MIMO system to identify the optimal AP cluster sizes. The AP cluster sizes 2 and 3 were found to be the optimal choices based on the median SINR value experienced by the UEs from the analysis performed. The integration of RIS to the MIMO and D-MIMO system models showed a huge improvement in the median SINR. From the study, it was observed that a conventional D-MIMO system outperforms a RIS-integrated MIMO system in terms of median SINR at UEs. The results from the SINR analysis also showed that the RIS-assisted D-MIMO system with a smaller AP cluster size and a sufficiently larger number of RIS elements outperformed a conventional D-MIMO system with a comparatively larger AP cluster size.

The results obtained from the average energy efficiency analysis of the RIS-assisted MIMO and D-MIMO system models w.r.t. the number of RIS elements proves the potential of RIS in improving the system's energy efficiency. From the results obtained, it was concluded that, for the indoor setup studied, as we move from a RIS-assisted MIMO system to a RIS-assisted D-MIMO system, the energy efficiency improvement becomes negligible. This is due to the multi-AP serving scenario in the D-MIMO system, which leads to a larger overall system power consumption. These results show the trade-off between the received data rate at UEs and the system's total power consumption.

The service coverage analysis w.r.t. the number of RIS elements also supports the potential of integrating passive RIS in an indoor D-MIMO system for achieving a highly reliable system for 5G and beyond technologies in terms of service coverage. This analysis showed the positive impact an indoor MIMO and D-MIMO system can achieve with the integration of RIS. Even though the rate of increase of service coverage was more significant in the RIS-integrated MIMO system compared to the RIS-assisted D-MIMO system, the later had a huge gap in terms of overall service coverage of the system. In addition, the service coverage kept improving as we increased the AP cluster size of the RIS-assisted D-MIMO system by a unit value. Furthermore, the rate of increase in service coverage w.r.t. the number of RIS elements declined as we increased the AP cluster size.

Overall, we can conclude that the RIS integration to the D-MIMO system showed a positive outcome in terms of parameters including median SINR at the UEs, energy efficiency, and service coverage probability. This shows its potential to be integrated into 5G and beyond (6G) technologies.

6
Future work

The future research plans include:

- To study partitioned RIS for a simultaneous and independent serving of multiple UEs which requires self-interference mitigation strategies to be investigated.
- To investigate the possibility of compensating an AP by a low-cost and energy-efficient RIS in a multi-AP serving D-MIMO system which could open up a new path of possibilities.
- To implement the RIS-integrated D-MIMO system in an outdoor scenario to study if it is worth deploying RIS in an outdoor D-MIMO system considering the influence of outdoor environmental factors.
- To study the multi-RIS assisted AP cluster scenario for the D-MIMO system to determine the optimal value of RIS cluster size that can serve the UEs in a system.

Bibliography

[1] O. Haliloglu et al., "Distributed MIMO Systems for 6G," 2023 Joint European Conference on Networks and Communications & 6G Summit (EuCNC/6G Summit), Gothenburg, Sweden, 2023, pp. 156-161, doi: 10.1109/EuCNC/6GSummit58263.2023.10188355.

[2] J. Sang et al., "Coverage Enhancement by Deploying RIS in 5G Commercial Mobile Networks: Field Trials," in IEEE Wireless Communications, vol. 31, no. 1, pp. 172-180, February 2024, doi: 10.1109/MWC.011.2200356.

[3] F. Zhu, Y. Zhao, W. Xu and X. You, "CSIT-Free Model Aggregation for Multi-RIS-Assisted Over-the-Air Computation," 2022 International Symposium on Wireless Communication Systems (ISWCS), Hangzhou, China, 2022, pp. 1-5, doi: 10.1109/ISWCS56560.2022.9940351.

[4] A. Zappone, M. Di Renzo and R. K. Fotock, "Surface-Based Techniques for IoT Networks: Opportunities and Challenges," in IEEE Internet of Things Magazine, vol. 5, no. 4, pp. 72-77, December 2022, doi: 10.1109/IOTM.001.2200170.

[5] M. Mercuri, E. Arnieri, R. De Marco, P. Veltri, F. Crupi and L. Boccia, "Reconfigurable Intelligent Surface-Aided Indoor Radar Monitoring: A Feasibility Study," in IEEE Journal of Electromagnetics, RF and Microwaves in Medicine and Biology, vol. 7, no. 4, pp. 354-364, Dec. 2023, doi: 10.1109/JERM.2023.3298730.

[6] E. C. Strinati et al., "Wireless Environment as a Service Enabled by Reconfigurable Intelligent Surfaces: The RISE-6G Perspective," 2021 Joint European Conference on Networks and Communications & 6G Summit (EuCNC/6G Summit), Porto, Portugal, 2021, pp. 562-567, doi: 10.1109/EuCNC/6GSummit51104.2021.9482474.

[7] M. A. Uusitalo et al., "6G Vision, Value, Use Cases and Technologies From European 6G Flagship Project Hexa-X," in IEEE Access, vol. 9, pp. 160004-160020, 2021, doi: 10.1109/ACCESS.2021.3130030.

[8] Ibrahim A. Haroun, "Introduction to MIMO and Beamforming Technology," in Essentials of RF Front-end Design and Testing: A Practical Guide for Wireless Systems , IEEE, 2024, pp.207-222, doi: 10.1002/9781394210640.ch8.

[9] Andreas F. Molisch, "Channel Models," in Wireless Communications , IEEE, 2011, pp.125-143, doi: 10.1002/9781119992806.ch7.

[10] T. S. Rappaport, Y. Xing, G. R. MacCartney, A. F. Molisch, E. Mellios and J. Zhang, "Overview of Millimeter Wave Communications for Fifth-Generation (5G) Wireless Networks—With a Focus on Propagation Models," in IEEE Transactions on Antennas and Propagation, vol. 65, no. 12, pp. 6213-6230, Dec. 2017, doi: 10.1109/TAP.2017.2734243.

[11] 3GPP TR 38.901 version 16.1.0 Release 16, 5G; Study on channel model for frequencies from 0.5 to 100 GHz

[12] Z. Li, H. Hu, J. Zhang and J. Zhang, "Enhancing Indoor mmWave Wireless Coverage: Small-Cell Densification or Reconfigurable Intelligent Surfaces Deployment?," in IEEE Wireless Communications Letters, vol. 10, no. 11, pp. 2547-2551, Nov. 2021, doi: 10.1109/LWC.2021.3106821.

[13] C. Huang, A. Zappone, G. C. Alexandropoulos, M. Debbah and C. Yuen, "Reconfigurable Intelligent Surfaces for Energy Efficiency in Wireless Communication," in IEEE Transactions on Wireless Communications, vol. 18, no. 8, pp. 4157-4170, Aug. 2019, doi: 10.1109/TWC.2019.2922609.

[14] A. Zappone and M. D. Renzo, "Energy Efficiency Optimization of Reconfigurable Intelligent Surfaces With Electromagnetic Field Exposure Constraints," in IEEE Signal Processing Letters, vol. 29, pp. 1447-1451, 2022, doi: 10.1109/LSP.2022.3181532.

[15] T. S. Rappaport, Y. Xing, G. R. MacCartney, A. F. Molisch, E. Mellios and J. Zhang, "Overview of Millimeter Wave Communications for Fifth-Generation (5G) Wireless Networks—With a Focus on Propagation Models," in IEEE Transactions on Antennas and Propagation, vol. 65, no. 12, pp. 6213-6230, Dec. 2017, doi: 10.1109/TAP.2017.2734243.

[16] W. Wang and E. S. Lohan, "Applicability of 3GPP Indoor Hotspot Models to the Industrial Environments," 2018 8th International Conference on Localization and GNSS (ICL-GNSS), Guimaraes, Portugal, 2018, pp. 1-5, doi: 10.1109/ICL-GNSS.2018.8440902.

[17] A. Zappone, M. Di Renzo, F. Shams, X. Qian and M. Debbah, "Overhead-Aware Design of Reconfigurable Intelligent Surfaces in Smart Radio Environments," in IEEE Transactions on Wireless Communications, vol. 20, no. 1, pp. 126-141, Jan. 2021, doi: 10.1109/TWC.2020.3023578.

[18] Q. Ye, O. Y. Bursalioglu, H. C. Papadopoulos, C. Caramanis and J. G. Andrews, "User Association and Interference Management in Massive MIMO HetNets," in IEEE Transactions on Communications, vol. 64, no. 5, pp. 2049-2065, May 2016, doi: 10.1109/TCOMM.2016.2547956.

[19] J. Wang, W. Tang, S. Jin, X. Li and M. Matthaiou, "Static Power Consumption Modeling and Measurement of Reconfigurable Intelligent Surfaces," 2023 31st European Signal Processing Conference (EUSIPCO), Helsinki, Finland, 2023, pp. 890-894, doi: 10.23919/EUSIPCO58844.2023.10289855.

DEPARTMENT OF ELECTRICAL ENGINEERING
CHALMERS UNIVERSITY OF TECHNOLOGY
Gothenburg, Sweden
www.chalmers.se

CHALMERS
UNIVERSITY OF TECHNOLOGY